Published in final edited form as:

*FASEB J.* 2021 August ; 35(8): e21771. doi:10.1096/fj.202100361R.

# PINK1 induced phosphorylation of mitofusin 2 (Mfn2) at serine 442 causes its proteasomal degradation and promotes cell proliferation in lung cancer and pulmonary arterial hypertension

**Asish Dasgupta**[#1], **Kuang-Hueih Chen**[#1], **Patricia D.A. Lima**[2], **Jeffrey Mewburn**[1], **Danchen Wu**[1], **Ruaa Al-Qazazi**[1], **Oliver Jones**[2], **Lian Tian**[1,4], **Francois Potus**[1,3], **Sebastien Bonnet**[3], **Stephen L. Archer**[1,2]

[1]Department of Medicine, Queen's University, Kingston, Ontario, K7L 3N6, Canada

[2]Queen's Cardiopulmonary Unit (QCPU), Translational Institute of Medicine (TIME), Department of Medicine, Queen's University, Kingston, Ontario, K7L 3N6, Canada

[3]Pulmonary Hypertension Research Group of the University Cardiology and Pulmonary Institute of the Quebec Research Centre, Laval University, Quebec City, Quebec, Canada.

[4]Strathclyde Institute of Pharmacy and Biomedical Sciences, University of Strathclyde, Glasgow, UK

[#] These authors contributed equally to this work.

## Abstract

Impaired mitochondrial fusion, due in part to decreased mitofusin 2 (Mfn2) expression, contributes to unrestricted cell proliferation and apoptosis-resistance in hyperproliferative diseases like pulmonary arterial hypertension (PAH) and non-small cell lung cancer (NSCLC). We hypothesized that Mfn2 levels are reduced due to increased proteasomal degradation of Mfn2 triggered by its phosphorylation at serine 442 (S442) and investigated the potential kinase mediators. Mfn2 expression was decreased and Mfn2 S442 phosphorylation was increased in pulmonary artery smooth muscle cells from PAH patients and in NSCLC cells. Mfn2 phosphorylation was mediated by PINK1 and protein kinase A (PKA), although only PINK1 expression was increased in these diseases. We designed a S442 phosphorylation deficient Mfn2 construct (PD-Mfn2) and a S442 constitutively phosphorylated Mfn2 construct (CP-Mfn2). The effects of these modified Mfn2 constructs on Mfn2 expression and biological function were compared with those of the wildtype Mfn2 construct (WT-Mfn2). WT-Mfn2 increased Mfn2 expression and mitochondrial fusion in both PAH and NSCLC cells resulting in increased apoptosis and decreased cell proliferation. Compared to WT-Mfn2, PD-Mfn2 caused greater Mfn2 expression, suppression of proliferation, apoptosis induction and cell cycle arrest. Conversely, CP-Mfn2 caused only a small increase in Mfn2 expression and did not restore mitochondrial fusion,

**Address correspondence to: Stephen L. Archer MD. FRCP(C), FAHA, FACC, FRSC,** Elizabeth Smith Distinguished University Professor, Tier 1 Canada Research Chair (Mitochondrial Dynamics & Translational Medicine), Professor & Head Department of Medicine, Queen's University, Etherington Hall, Room 3041, 94 Stuart St., Kingston, Ontario, Canada, K7L 3N6, stephen.archer@queensu.ca, Telephone: 613 533-6327; Fax: 613 533-6695.

**Author's Contribution:** SLA conceived the study. AD, KHC, PDAL, JM, DW, RA, OJ, LT, FP, SB designed, executed and analyzed experiments. SLA supervised experimental studies. AD, KHC and SLA interpreted results and wrote the manuscript.

**Declaration of interests:** The authors declare no competing interests.

inhibit cell proliferation or induce apoptosis. Silencing PINK1 or PKA, or proteasome blockade using MG132, increased Mfn2 expression, enhanced mitochondrial fusion and induced apoptosis. In a xenotransplantation NSCLC model, PD-Mfn2 gene therapy caused greater tumor regression than did therapy with WT-Mfn2. Mfn2 deficiency in PAH and NSCLC reflects proteasomal degradation triggered by Mfn2-S442 phosphorylation by PINK1 and/or PKA. Inhibiting Mfn2 phosphorylation has potential therapeutic benefit in PAH and lung cancer.

### Keywords

Adenoviral gene therapy; phosphatase and tensin homolog (PTEN)-induced putative kinase 1 (PINK1); protein kinase A (PKA); mitochondrial dynamics; non-small cell lung cancer (NSCLC)

## Introduction:

Mitochondria exist in dynamic networks and are constantly dividing (fission) and joining together (fusion) through processes that are regulated by large GTPases, including the fission mediator, dynamin-related protein 1 (Drp1), and fusion mediators, which include mitofusin 1 (Mfn1) and mitofusin 2 (Mfn2) as well as optic atrophy 1 (OPA1) (1). In proliferating cells, mitochondrial fission and nuclear division are co-ordinated cellular processes. This coordination ensures equitable distribution of mitochondria between daughter cells, reviewed in (1). Mitotic fission, the division of mitochondria which accompanies mitosis, is mediated in part by coordinated activation of fission (by Drp1) and suppression of fusion (by Mfn2). In hyperproliferative diseases such as lung cancer and pulmonary arterial hypertension (PAH), a fatal cardiopulmonary disease, the balance between mitochondrial fission and fusion is dysregulated such that fission exceeds fusion (2, 3). These disorders of mitochondrial dynamics result in mitochondrial fragmentation, a newly recognized phenotypic hallmark of both diseases. Increased rates of mitotic fission favour rapid cell proliferation. In both cancer and PAH, mitochondrial fragmentation is due, in part, to the aggregate effects of downregulation of Mfn2 expression (3–7), post-translational increases in Drp1 activity (2, 8–10) and increases in the expression of Drp1's binding partners, MiD49 and MiD51 (11, 12). Inhibition of mitotic fission triggers cell cycle arrest and apoptosis. Thus, both excessive fission and impaired fusion are attractive therapeutic targets in hyperproliferative disorders (3, 11–13).

Hyperproliferative disorders, such as cancer and PAH, are characterized by excessive cell proliferation and resistance to apoptosis. The neoplastic phenotype of cancer and the pseudo-neoplastic phenotype of PAH are multifactorial but are due in part to disorders of mitochondrial dynamics (14). The activity of the large GTPases that mediate mitochondrial dynamics is largely regulated post-translationally by kinases and phosphatases (1). In both cancer and PAH, there is excessive mitochondrial fission, caused by post-translational activation of Drp1 (2, 3, 15–17). This Drp1 activation reflects differential phosphorylation of Drp1 at serine 616 and serine 637 by various protein kinases (2, 15, 18), as well as epigenetically mediated changes in expression of the partner proteins that bind activated Drp1 (11, 12). In hyperproliferative disorders, there is a corresponding decrease in mitochondrial fusion, due to decreased expression of Mfn2 (3, 4, 11, 12). Inhibition of Drp1

or augmentation of Mfn2 have been shown to regress experimental PAH and inhibit tumor growth in animal models (2, 3, 13).

However, the mechanism by which Mfn2 is downregulated in PAH and cancer is not fully understood. In this study, we determined whether post-translational modification of Mfn2, specifically its phosphorylation at serine 442 residue (S442), leads to Mfn2's proteasomal degradation and reduced expression in PAH and lung cancer. We also evaluated the role of two kinases that putatively phosphorylate Mfn2 at S442. This study is based on the observation that phosphatase and tensin homolog (PTEN)-induced putative kinase 1 (PINK1) can phosphorylate Mfn2 at S442, which may trigger proteasomal degradation of Mfn2 protein in murine cardiomyocytes and fibroblasts (19). Furthermore, *in silico* analysis showed that protein kinase A (PKA) is predicted to phosphorylate S442 of Mfn2. We also explored the possibility that PKA regulates Mfn2 expression through a similar proteasomal regulatory mechanism. Therefore, we explored the therapeutic benefit of targeting PINK1 and PKA to regulate Mfn2 phosphorylation and restore Mfn2 expression. Since PAH and cancer share a hyperproliferative and apoptosis resistant phenotype, we performed experiments in pulmonary arterial smooth muscle cells (PASMC) from patients with PAH and in cancer cells and xenotransplantation tumor models, using the A549 (non-small cell lung cancer, NSCLC) cell line.

We show that in both PAH and NSCLC, low Mfn2 levels result from increased PINK1 expression and are associated with increase in the phosphorylation of S442. In addition, inhibiting PINK1 or modifying the structure of Mfn2, to eliminate the phosphorylation potential of S442, preserves Mfn2 levels and inhibits the hyperproliferative, apoptosis-resistant phenotype in these syndromes. While PKA is not upregulated in PAH or NSCLC, manipulation of PKA activity regulates S442 phosphorylation and Mfn2 expression, indicating that PKA is also a potent regulator of this pathway. These findings identify the mechanisms of Mfn2 downregulation in two lethal human diseases and demonstrate potential therapeutic strategies to augment Mfn2.

## Materials and Methods:

### Cell culture:

PAH PASMC were isolated from PAH patients. Normal PASMC were isolated from control subjects or purchased from Lonza (Walkersville, MD, USA). PASMC lines were studied within 6 passages. PASMC were grown in Medium 231 supplemented with Smooth Muscle Growth Supplement (SMGS, Life Technologies, Carlsbad, CA, USA). Experiments were performed on 9 normal PASMC lines (67% Female, mean age: 46.1 years) and 11 PAH PASMC lines (55% Female, mean age: 43.1 years). Adenocarcinoma human alveolar basal epithelial cells, A549 were obtained from ATCC (Manassas, VA, USA). A549 cells were cultured in Dulbecco's modified Eagle's medium (DMEM) containing 10% FBS, 100 U/ml penicillin, 100 μg/ml streptomycin, and 2 mM glutamine and passaged every 3 days. The human non-neoplastic bronchial epithelial cells, BEAS-2B, was purchased from ATCC (Manassas, VA, USA) and cultured following the instructions by ATCC. Normal human bronchial epithelial cells (NHBE), as well as their culture medium, were purchased from Lonza (Walkersville, MD, USA).

### Viral constructs and siRNA:

Construction of the Mfn2 mutants was performed by site-directed mutagenesis using the pCR8/CMV/TOPO/Mfn2 plasmid as double-stranded template and the QuickChange II XL site-directed mutagenesis kit (Stratagene, USA). To construct the phosphodeficient mutant (PD-Mfn2), we replaced serine with alanine at residue 442 of Mfn2: 5-GAA GAG ATC AGG CGC CTC GCA GTG CTG GTT GAC GAG TAC-3, 5-GTA CTC GTC AAC CAG CAC TGC GAG GCG CCT GAT CTC TTC-3. To construct the phosphomimetic mutant (CP-Mfn2), we replaced serine with aspartic acid at residue 442 of Mfn2: 5-GAA GAG ATC AGG CGC CTC GAC GTG CTG GTT GAC GAG TAC-3, 5-GTA CTC GTC AAC CAG CAC GTC GAG GCG CCT GAT CTC TTC-3. Alanine provided a non-phosphorylatable non-polar residue with minimal structural change to the protein, while the aspartic acid residue provided a constitutive negative charge to mimic phosphorylation.

After mutagenesis, adenoviruses were produced by recombining the mutated plasmids with the Gateway-adapted destination vector, pAd/CMV/V5-DEST, using the ViraPower Adenoviral expression system (Invitrogen, Carlsbad, CA, USA) and packaging the constructs in 293A cells. Viral particles were purified by cesium chloride (Sigma-Aldrich, St. Louis, MO, USA) density gradient centrifugation. The titer of the virus stock was expressed as plaque forming units (pfu). The two adenoviruses with mutated Mfn2 were designated Adv-Mfn2-S442A (PD-Mfn2) and Adv-Mfn2-S442D (CP-Mfn2). Adenoviral infection was carried out by infection with Adv-WT-Mfn2, Adv-PD-Mfn2 or Adv-CP-Mfn2 or adenovirus expressing bacterial-galactosidase (Adv-LacZ) as a control. siPINK1 (Cat # 4390824) was purchased from Ambion Inc. (Foster City, CA). siPKA C-α (Cat # 6574S) was purchased from Cell Signaling Technology (Beverly, MA, USA). For siRNA transfection, cells were grown to 80% confluence and then transfected with 25 picomole of siRNA using the Lipofectamine® *RNAiMAX* Transfection Reagent (Life Technologies, Carlsbad, CA). The knockdown efficiency was assessed after 48 hours of transfection using qRT-PCR (Bio-Rad, Hercules, CA, USA) or after 72 hours of transfection using immunoblotting.

### Adenoviral infection:

Cells were plated in 6-well plates and incubated overnight at 37°C. When the cells reached optimal confluency, the cells were counted and infected with the indicated adenoviruses at 100 pfu/cell at 37°C. The cells were then analyzed after 48 or 72 hours, depending on the assay performed.

### Antibodies and Reagents:

Polyclonal antibody against Mfn2 (M-6444) was purchased from Sigma-Aldrich (St. Louis, MO, USA) and the monoclonal antibody against Mfn2 (ab56889) was purchased from Abcam (Cambridge, MA, USA), respectively. The antibody targeting p-Mfn2$_{S442}$ (ABC963) was obtained from Millipore (Burlington, MA, USA). Since there is lack of antibody specificity in direct detection of p-Mfn2$_{S442}$ by immunoblotting, we immunoprecipitated total Mfn2 and probed it with the p-Mfn2$_{S442}$ antibody. This procedure gave us a more specific binding of Mfn2. Antibodies specific for PINK1 (6494S and ab23707) were obtained from Cell Signalling Technology (Beverly, MA, USA) and Abcam (Cambridge,

MA, USA) respectively. Antibodies against LC3B (2775S) and PCNA (1310) were obtained from Cell Signalling Technology (Beverly, MA, USA). Antibodies against PKA C-α (4782) and GAPDH (5174S) were also obtained from Cell Signalling Technology. The PKA specific inhibitors Rp-cAMPS (BML-CN135–0001) and PKI (CAS99534–03-9) were purchased from Enzo Life Sciences (Farmingdale, NY, USA) and Santa Cruz Biotechnologies (Dallas, TX, USA), respectively. The proteasome inhibitor MG132 was purchased from Enzo Life Sciences (BML-PI102–0025). Secondary antibodies, goat anti-rabbit Alexa Fluor 488 (011038) and goat anti-mouse Alexa Fluor 546 ( A11003) were obtained from Life Technologies (Carlsbad, California, USA).

### Immunoblotting:

Whole-cell lysates were prepared in cell signaling lysis buffer (Cell Signaling Technologies, Beverly, MA, USA). For immunoblot analysis, 40–60 μg of cell lysates was analyzed on a 4–12% NuPAGE gel (Life Technologies, Carlsbad, CA, USA). The proteins were electrotransferred to PVDF membranes (Life Technologies, Carlsbad, CA, USA), and detection of specific proteins was carried out with indicated antibodies using an ECL-Plus Western Blotting Detection System (GE Healthcare, Piscataway, NJ, USA).

### Immunofluorescence staining:

Blocks were sectioned at 4μm thickness and baked at 60$^{o}$C for 2 hours to adhere them to the slides. Deparaffinization was performed with 3 changes of xylene for 5 minutes each, then rehydration was performed using graded ethanol (100% twice, 95%, 70% for 5 minutes each) before the slide was exposed to running tap water for 5 minutes. Heat induced epitope retrieval was done using Tris-EDTA buffer at pH 9.0, using a microwave pressure cooker for 4 minutes. The sections were incubated with the primary antibodies overnight at 4$^{o}$C, then washed in PBS for 3 times. Secondary antibodies were added for 1 hour at room temperature and then rinsed in PBS 3 times, before mounting with anti-fade DAPI mounting medium.

### Immunoprecipitation:

Cell pellets were lysed with cell signaling lysis buffer (Cell Signaling Technologies, Beverly, MA, USA) supplemented with a protease and phosphatase inhibitor cocktail (Thermo Fisher Scientific, Waltham, MA, USA). Immunoprecipitation reactions were performed by incubating the cell lysates with a polyclonal anti-Mfn2 antibody at 4$^{o}$C overnight. The immune complexes were recovered by incubation with protein A/G-PLUS agarose (Santa Cruz Biotechnology, Dallas, TX, USA). After washing with buffer, the beads were boiled in NuPAGE sample buffer (Invitrogen, Carlsbad, CA, USA) to elute the bound protein and immunoprecipitated proteins were analysed by immunoblotting (20).

### Cell cycle analysis:

PAH PASMC or A549 cells were infected with serotype 5 adenoviruses carrying the indicated Mfn2 constructs for 24 hours at 100 pfu/cell. Following adenoviral infection, the cells were serum starved for 48 hours to achieve cell cycle synchronization and then stimulated with 10% FBS for 20 hours (for A549 cells) or 15% FBS for 24 hours (for PAH PASMC). Cells were harvested, resuspended in 300 μl 1× phosphate-buffered saline (PBS),

and fixed with 70% ethanol (v/v) at −20°C. The fixed cells were washed with ice cold PBS and incubated with 500 μl of propidium iodide (PI)/staining buffer (BD Biosciences, Franklin Lakes, NJ, USA) at room temperature for 15 minutes. The samples were analyzed for DNA content using flow cytometry to detect PI binding to DNA using the SONY fluorescence-activated cell sorter (Sony SH-800, San Jose, CA, USA).

### Cell proliferation:

Cell proliferation was quantified in triplicate using the Click-iT EdU kit (C10420) according to the manufacturer's instructions (Life Technologies, Carlsbad, CA, USA). Measurements were made 72 hours following infection of the cells by the indicated adenoviruses at 100 pfu/cell.

### Apoptosis Assay:

Apoptosis was quantified by the Cell Death ELISA (Roche Applied Science, Penzberg, Germany) or by Alexa Fluor 488 Annexin V/Dead Cell Apoptosis Kit (Life Technologies, Carlsbad, CA, USA). Cells were infected with adenoviruses carrying indicated Mfn2 constructs at 100 pfu/cell or transfected by siRNAs against PINK1 or PKA C-α. The apoptosis assays were performed 72 hours following adenoviral infection or siRNA transfection, following the manufacture's instruction.

### Mitochondrial imaging and quantification of fission:

Cells grown in glass-bottom dishes were infected with adenoviruses carrying the indicated Mfn2 constructs or siRNAs against PINK1 or PKA C-α or PKA inhibitors. 48 hours following transfection, the cells were loaded with the mitochondrial potentiometric dye, tetramethylrhodamine (TMRM; 50 nM, 20 minutes in culture medium at 37°C; Molecular Probes, Eugene, OR, USA) or stained with Mitotracker Green (Thermo Fisher Scientific, Waltham, MA, USA). Cells were imaged with the Leica SP8 confocal laser scanning microscope using a 1.40 NA, 63× oil immersion objective with ×1.5 digital zoom (TMRM: excitation at 561 nm, emission recorded above 575 nm; Mitotracker Green: excitation at 490 nm, emission recorded above 516 nm; Leica Planapo, Wetzlar, Germany). Continuous mitochondrial structures were counted with ImageJ's particle counting subroutine and the number was normalized to the total mitochondrial area to obtain the mitochondrial fragmentation count (MFC) for each image, a previously described metric (3). For every intervention, 9–59 randomly selected cells were imaged by a microscopist who was blinded to treatment group. A decrease in MFC indicates a more fused mitochondrial network, as previously described (11–13).

### Mitochondrial ROS production:

Cells were infected with adenoviruses carrying the indicated Mfn2 constructs at 100 pfu/cell. 48 hours post infection, the cells were stained with MitoSOX™ Red Mitochondrial Superoxide Indicator (Invitrogen, Carlsbad, CA, USA), following manufacturer's instructions, and imaged with Leica SP8 confocal laser scanning microscope (Leica Planapo, Wetzlar, Germany).

### Pyruvate dehydrogenase (PDH) activity assay:

Cells were infected with adenoviruses carrying LacZ or PD-Mfn2 constructs at 100 pfu/cell. PDH activity was measured 48 hours post infection by the PDH colorimetric activity assay kit (Sigma Aldrich, St Louis, MO, USA) following manufacturer's instructions.

### Machine learning to quantify mitochondrial fusion:

A machine-learning based categorization was used for further analysis of mitochondrial morphology using Leica LAS X software, as previously described (11). Briefly, every mitochondrion in each cell was categorized as punctate, intermediate or filamentous, using an algorithm calculated based on mitochondrial area, length and sphericity. Initially, 15–20 mitochondria were manually selected from each category to inform the machine-learning algorithm. The algorithm was then applied to all subsequent images and the percentage area of each category in each confocal image was calculated automatically.

### Preparation of monocrotaline (MCT)-PAH rodent model:

MCT induced PAH model in rats was created by subcutaneous injection of 60mg/kg of MCT, as previously described (21).

### *In vivo* xenograft tumor models:

BALB/c-Rag2$^{-/-}\gamma c^{-/-}$ (5–6 weeks old) mice were housed in the Queen's University Animal Care Facility. All the animal experiments and procedures conformed to the institutional animal care guidelines (protocol number: 1902). A xenograft model of human NSCLC was established in BALB/c-Rag2$^{-/-}\gamma c^{-/-}$ mice by a dorsal subcutaneous injection of A549 cells (3–4 $\times 10^6$ cells) as previously described (12). When the tumors reached ~5 mm diameter (usually 2-weeks after xenotransplantation), therapies were initiated. For Adv-Mfn2 treatments, $1 \times 10^9$ pfu (0.1 ml) virus/tumor was injected. An equivalent dose of Adv-LacZ was used as control therapy. Tumor size was measured every 4 days using a Vernier caliper. At the end of the study (approximately 2 weeks following initiation of therapy), the mice were euthanized, and the tumors were removed. The tumor weight was measured, and the volume of the tumors was calculated as described previously (12).

### Statistical analyses:

Quantitative data are presented as mean ± SEM. Intergroup differences were assessed using Students' t-test or Mann-Whitney U test as appropriate. One-way ANOVA was used to compare the means of three or more independent groups. For intergroup comparison of mitochondrial categories, two-way ANOVA was used. Statistical analyses were performed using the GraphPad Prism 8.0d software package (San Diego, CA, USA). A $P < 0.05$ was considered statistically significant.

### Materials and Correspondence:

Correspondence and material requests should be addressed to Stephen L. Archer.

### Data and material availability:

All data associated with this study are available in the main text or in the supplementary materials.

## Results:

### Mfn2 is downregulated in PAH and lung cancer

Cells from hyperproliferative disease origin, such as PASMC isolated from PAH patients and A549 NSCLC cells, have fragmented mitochondria relative to appropriate normal control cells (2, 3) (also see Supplementary Figure 8). Immunoblot analyses of human control PASMC versus PAH PASMC revealed decreased expression of Mfn2 in PAH PASMC (Fig. 1A). A similar downregulation of Mfn2 was observed in A549 cells compared to normal bronchial epithelial cells (NHBE) or a non-neoplastic bronchial epithelial cell line, BEAS-2B (Fig. 1B–C).

### Augmenting Mfn2 inhibits proliferation in PAH PASMC and A549 cells

Overexpressing WT-Mfn2 significantly inhibited cell proliferation in PAH PASMC and A549 cells (Fig. 2A–B). In contrast, silencing Mfn2 in normal human PASMC, using siRNA, increased cell proliferation, creating a PAH phenotype (Fig. 2C).

### PINK1 is involved in the degradation of Mfn2 in PAH PASMC and A549 cells

The S442 of Mfn2 is a site for PINK1 phosphorylation (19). Phosphorylation of Mfn2's S442 by PINK1 leads to parkin-mediated ubiquitination and subsequent degradation of Mfn2 (19). Therefore, we assessed the expression of PINK1 in PAH PASMC and A549 cells compared to their respective normal controls. As shown in Fig. 3A and Supplementary Figure 1A, the expression of PINK1 was markedly increased in PAH PASMCs. Furthermore, we observed a strong negative correlation between the protein expression of Mfn2 and the expression of PINK1 in human PASMC (Fig. 3B). In addition, we observed a positive correlation between the expression of PINK 1 and proliferation and a negative correlation between Mfn2 expression and proliferation in normal and PAH PASMC (Supplementary Figure 1B–D). The expression of PINK1 was also found to be increased in the pulmonary arterioles from rats with MCT-PAH (Supplementary Figure 1E). The expression of PINK1 was also elevated in A549 cells when compared to control cells (NHBE and BEAS-2B cells) (Fig. 3C–D). Furthermore, we observed a positive correlation between the expression of PINK 1 and proliferation and a negative correlation between Mfn2 expression and proliferation in BEAS-2B and A549 cells (Supplementary Figure 1F–H). If PINK1 is responsible for the degradation of Mfn2, then silencing PINK1 should induce mitochondrial fusion by upregulating Mfn2 expression. As shown in Fig. 3E–J and Supplementary Figure 2, knocking down PINK1 upregulated Mfn2 expression and induced mitochondrial fusion in both PAH PASMC and A549 cells. Furthermore, silencing PINK1 inhibited cell proliferation and induced apoptosis in both PAH PASMC and A549 cells (Fig. 3K–N).

In silico data-mining suggested PKA as an additional candidate kinase that might phosphorylate Mfn2's S442 (Supplementary Figure 3A–B). Therefore, we also tested whether PKA-mediated phosphorylation of Mfn2 makes it a target for proteasomal

degradation. Were this the case, then inhibiting PKA should block the degradation of Mfn2. To test this hypothesis, we treated A549 cells with a PKA inhibitor, Rp-cAMPS. As shown in Fig. 3O, this specific PKA inhibitor upregulated the expression of Mfn2. To further confirm the involvement of PKA in the downregulation of Mfn2, we treated the A549 cells with another PKA-specific synthetic peptide inhibitor, PKI. As shown in Fig. 3P, Mfn2 was upregulated in a dose-dependent manner by PKI. The effect of upregulation of Mfn2 by PKA inhibition was evidenced by the restoration of a more fused mitochondrial morphology in A549 cells by Rp-cAMPS treatment (Fig. 3Q–R). Rp-cAMPS treatment also inhibited the proliferation of PAH PASMC (Supplementary Figure 4).

If inhibiting PKA upregulates Mfn2 and increases mitochondrial fusion, then blocking PKA activity should also inhibit cell proliferation. To test this hypothesis, we successfully knocked down PKA using siRNA against PKA C-α, one of the isoforms of the catalytic subunit of PKA in A549 cells. Silencing PKA C-α resulted in the upregulation of Mfn2 and restored a fused mitochondrial morphology (Fig. 3S–V). Silencing PKA C-α also inhibited cell proliferation and increased apoptosis (Fig. 3W–X). In addition, we observed that silencing PKA C-α increased the expression of cleaved LC3B indicating an increase in mitophagy and upregulation of Mfn2 expression. Likewise, lysosomal inhibition by Bafilomycin A1 downregulated Mfn2 expression. Taken together these results indicate that upregulation of Mfn2 by PKA silencing is not due to blockade of mitophagy or lysosomal inhibition (Supplementary Figure 5A–B).

### S442 phosphorylation of Mfn2 is increased in PAH PASMC and NSCLC cells

We next observed higher levels of Mfn2 phosphorylation at S442 in both PAH PASMC and A549 cells, compared to their normal counterparts (Fig. 4A–B). Moreover, silencing PINK1 inhibited phosphorylation of Mfn2 at S442 (Fig. 4C–D). These experiments confirm a role of endogenously upregulated PINK1 in phosphorylating Mfn2 at S442. Although PKA expression was not increased in PAH PASMC or A549 cells (Supplementary Figure 6A–B), we did observe a decrease in Mfn2 phosphorylation at S442 residue when PKA C-α was knocked down in A549 cells (Fig. 4E).

### Increased expression of Mfn2 post PD-Mfn2 treatment compared to WT-Mfn2

To determine the role of S442 phosphorylation in Mfn2's proteasomal degradation, we generated two new Mfn2 constructs: 1) S442 was replaced with alanine, yielding a phosphodeficient (PD) mutant (Mfn2-S442A); 2) S442 was replaced with aspartic acid, creating a mutant that mimics a constitutively phosphorylated (CP) variant (Mfn2-S442D). We then established a comprehensive Mfn2 expression profile of wildtype (WT), PD and CP-Mfn2. The PAH PASMC and A549 cells were infected with adenoviruses carrying the indicated Mfn2 constructs. The results showed a significant increase in the expressions of Mfn2 with PD-Mfn2 compared to the WT-Mfn2. CP-Mfn2 failed to substantially increase Mfn2 expression (Fig. 5A–B).

### Involvement of proteasome in the downregulation of Mfn2

To investigate the possibility of the involvement of the proteasome in the decreased expression of Mfn2 with CP-Mfn2, A549 and PAH PASMC were infected with adenovirus

carrying CP-Mfn2 constructs. After 40 hours of infection, the cells were treated with a proteasome inhibitor, MG132 for 8 hours. MG132 successfully blocked the degradation of CP-Mfn2, indicating the involvement of proteasome in the degradation of CP-Mfn2 in A549 and PAH PASMC (Fig. 5C and Supplementary Figure 7A–B).

### Restoring Mfn2 expression increases mitochondrial fusion in PAH PASMC and A549 cells

PAH PASMC and A549 cells have fragmented mitochondrial networks compared to their normal counterparts (Supplementary Figure 8), as previously reported (2). PD-Mfn2 increased mitochondrial fusion more than WT-Mfn2 whilst CP-Mfn2 had no effect on the mitochondrial fragmentation, as shown in the representative images, by quantification of the mitochondrial fragmentation count (MFC) and by a previously validated machine-learning automated algorithm that measures the percentage area of filamentous mitochondria (Fig. 5D–G).

### PD-Mfn2 is more effective than WT-Mfn2 in inhibiting proliferation and inducing apoptosis in PAH PASMC and A549 cells

WT-Mfn2 inhibits cell proliferation in vascular smooth muscle cells and cancer cells (4, 20, 22). If phosphorylation of S442 of Mfn2 is, at least in part, responsible for Mfn2 degradation, rendering it phosphorylation resistant should enhance both its expression level and antiproliferative potency. In contrast, the phospho-mimetic form of Mfn2 (CP-Mfn2) would be predicted to have little or no effect on Mfn2 expression level or cell proliferation. To test this hypothesis, we overexpressed the indicated Mfn2 constructs by adenoviral-mediated gene transfer in PAH PASMC and A549 cells. As anticipated, PD-Mfn2 not only increased Mfn2 expression to higher levels than WT-Mfn2 (Fig. 5A–B) but also achieved an 84% and 52% suppression of cell proliferation in PAH PASMC and A549 cells, respectively; compared to a 45% and 31% suppression of proliferation in PAH PASMC and A549 cells respectively, by WT-Mfn2 (Fig. 5H–I). In contrast, CP-Mfn2, which failed to increase Mfn2 expression (Fig. 5A–B), also failed to inhibit cell proliferation in both PAH PASMC and A549 cells (Fig. 5H–I). We also observed an inverse correlation between Mfn2 expression and proliferation of PAH PASMC and A549 cells augmented with indicated Mfn2 constructs (Supplementary Figure 9A–B). Furthermore, we observed a significant increase in mitochondrial ROS and PDH activity by PD-Mfn2 in A549 cells (Supplementary Figure 9C–D).

PAH and cancer cells are characterized by apoptosis resistance (4, 23). Therefore, induction of apoptosis could be one of the ways to target these hyperproliferative cells. There was a significant increase in the rate of unstimulated apoptosis in WT-Mfn2 overexpressed cells as compared to the LacZ control in PASMC and A549 cells respectively, (Fig. 5J–K). However, the induction of unstimulated apoptosis was greater in PD-Mfn2 infected cells compared to WT-Mfn2 (Fig. 5J–K). CP-Mfn2 failed to induce apoptosis (Fig. 5J–K). These data support the hypothesis that restoring Mfn2 level increases apoptosis in PAH and cancer cells and show that a designer form of Mfn2, which is resistant to proteasomal degradation, is most effective.

### PD-Mfn2 induces cell cycle arrest in the G0/G1 phase

To test the effects of the Mfn2 constructs on cell cycle, PAH PASMC and A549 cells were infected with adenoviruses carrying the indicated Mfn2 constructs and the distribution of cells in different phases of the cell cycle was then determined. Following release from the synchronization (achieved by serum deprivation), WT-Mfn2 overexpressed cells manifested G1/G0 arrest; however, the greatest degree of cell cycle blockade at G1/G0 phase was observed in PD-Mfn2 overexpressing cells (Fig. 6A–B). These data support the notion that mitotic fission is required for cell cycle progression and confirm a role of Mfn2 in this mitochondrial regulated proliferation pathway.

### Xenotransplantation model of NSCLC

We explored the therapeutic implications of restoring Mfn2 expression in a xenotransplant murine model of cancer. Adv-PD-Mfn2 treatment reduced tumor volume by 69% when compared to the tumor volume in Adv-LacZ infected tumors (Fig. 7A–B). Furthermore, a 56% reduction in tumor volume was observed in Adv-PD-Mfn2 treated tumors when compared to the Adv-WT-Mfn2 treated tumors (Fig. 7A–B). We further observed a 60% reduction of tumor weight with Adv-PD-Mfn2 treatment as compared to the tumors treated with Adv-WT-Mfn2 (Fig. 7C). In addition, we observed a decrease in PCNA/Mfn2 ratio in WT-Mfn2 treated tumors which was further decreased in Adv-PD-Mfn2 treated tumors compared to the Adv-LacZ control, suggesting a superior inhibition of tumor growth by PD-Mfn2 relative to WT-Mfn2 (Fig. 7D and Supplementary Figure 10).

## Discussion

This study identifies an important and therapeutically tractable mechanism underlying the deficiency of Mfn2 that is commonly observed in proliferative disorders which contributes to rapid cell proliferation and impaired apoptosis in PAH and NSCLC (3, 4). We show that downregulation of Mfn2 is induced by proteasomal degradation triggered by PINK1, which phosphorylates Mfn2 at S442. PINK1 is upregulated in both human PAH PASMC and lung cancer cells. In addition, the expression levels of PINK1 and Mfn2 are inversely correlated in both PAH and lung cancer cells, consistent with our molecular studies showing that PINK1 drives Mfn2 phosphorylation and degradation (Fig. 3B). The consequences of accelerated proteasomal degradation of Mfn2 include a fragmented mitochondrial network which permits increased mitotic fission and supports rapid cell proliferation. Evidence for this conclusion includes the observation that inhibiting phosphorylation at S442 of Mfn2 increases Mfn2 expression, restores a fused mitochondrial network and causes G0/G1 cell cycle arrest in both PAH and cancer cells. Although PINK1 appears to be the primary endogenous regulator of Mfn2 levels, PKA is also able to modulate S442 phosphorylation and PKA inhibition (molecular or pharmacologic) can restore Mfn2 expression. Finally, we show the therapeutic potential of this discovery by demonstrating that a variant of Mfn2, engineered to be phospho-deficient (PD-Mfn2), has improved ability to elevate Mfn2 expression and an associated enhanced antiproliferative/proapoptotic effects in both PAH PASMC and lung cancer cells *in vitro*. We also report that PD-Mfn2 is superior to WT-Mfn2 in rescuing mitochondrial morphology and has greater therapeutic benefit in the xenotransplantation murine model of lung cancer.

Dysregulation of the balance between mitochondrial fusion and fission, in which fission exceeds fusion, contributes to excessive mitochondrial fragmentation in PAH and many cancers. This novel hallmark of hyperproliferative cells has been identified and confirmed by several studies and has been targeted with therapeutic benefits in preclinical studies (2, 3, 11, 12). This abnormality of mitochondrial structure is reflective of a disturbance of mitotic fission and functionally is permissive of an imbalance favoring proliferation and impaired apoptosis in proliferating cells (1). This imbalance between mitochondrial fission and fusion in PAH and cancer is multifactorial, caused by upregulation and activation of the fission mediator Drp1, upregulation of Drp1 binding partners, MiD49 and MiD51 (11, 12), and the downregulation/inactivation of the fusion proteins Mfn1 and Mfn2 (3, 4).

The molecular mechanism for the coordination of mitochondrial and nuclear division is not fully understood. Dysregulation of mitochondrial fusion, due to down-regulation of Mfn2 contributes to fragmented mitochondrial network (3). Mitochondrial fragmentation contributes to the hyperproliferative phenotype in several ways, such as by accelerating mitotic fission, a process allowing equitable distribution of mitochondria to daughter cells during mitosis (1). Mitochondrial fragmentation also interrupts intramitochondrial calcium waves, thereby preventing calcium-mediated apoptosis (25). Downregulation of Mfn2 has been reported in hyperproliferative diseases such as lung and gastric cancers and in PAH (3, 4, 26). The importance of Mfn2 deficiency to the hyperproliferative state in both benign cells (4, 20, 22) and tumors (3) is evident in that heterologous overexpression of Mfn2 suppresses cell proliferation. This occurs, in part, by Mfn2 binding Ras and thereby inhibiting the Ras-Raf-ERK1/2 signalling pathway (20, 22). Furthermore, overexpression of Mfn2 is proapoptotic, which is mediated by the inhibition of Akt signalling resulting in the activation of the mitochondrial apoptotic pathway (27).

In this study, we elucidate the physiological role of Mfn2 in normal cells, while emphasizing the impact of its downregulation in two hyperproliferative diseases. Likewise, we have replicated our prior finding of reduced Mfn2 expression in PAH PASMC (4) and in A549 cells (3) (Fig. 1A–C). Also as previously noted, augmenting Mfn2 inhibits proliferation of PAH PASMC and A549 cells while silencing Mfn2 in normal PASMC recapitulated a hyperproliferative phenotype (Fig. 2A–C), highlighting the role of Mfn2 in the regulation of mitotic fission.

Novel findings in the current study include demonstrating a major mechanism of Mfn2 downregulation (PINK1 phosphorylation of S442) and demonstrating the potential of this mechanism as a therapeutic target. The expression of Mfn2 is controlled both at transcriptional and post-translational levels. The transcription of Mfn2 is regulated by peroxisome proliferator-activated receptor γ coactivator-1 α (PGC-1α), the expression of which is downregulated in human and experimental PAH (4). At the post-translational level, Mfn2 is phosphorylated at S27 by c-Jun N-terminal kinase (JNK) in response to cellular stress, leading to the recruitment of the ubiquitin ligase (E3), Huwe1. This S27 phosphorylation leads to ubiquitin-mediated proteasomal degradation of Mfn2 (24). Mfn2 expression is also regulated by the PI3K-AKT-mTOR pathway in a proteasome-dependent manner, which plays a critical role in activation-induced downregulation of Mfn2 expression in resting human T-cells (25). Mfn2 has also been previously shown to be phosphorylated at

its S442 residue by PINK1 (19), which we confirm in the current study. This phosphorylation recruits the E3 ubiquitin ligase parkin to mitochondria thereby promoting ubiquitination of Mfn2 and its subsequent degradation (19). Our results reveal increased expression of PINK1 both in human and a rodent model of PAH (Fig. 3A and Supplementary Figure. 1A–B). Likewise, PINK1 is upregulated in A549 cells, an NSCLC cell line (Fig. 3C–D).

There is an inverse correlation between the expression of PINK1 and Mfn2 (Fig. 3A–B). This is expected since PINK1 promotes proteasomal degradation of Mfn2. Likewise, there is a positive correlation between PINK1 expression and rates of cell proliferation (Supplementary Figure 1C and Supplementary Figure 1G). In contrast, there is an inverse correlation between Mfn2 expression and cell proliferation (Supplementary Figure 1D and Supplementary Figure 1H). These correlations are consistent with our other findings and indicate that PINK1 is a negative regulator of Mfn2 and that Mfn2 is an inhibitor of cell proliferation. Therefore, we conclude that it is the pathological upregulation of PINK1 that predominantly mediates Mfn2 downregulation, leading to excessive mitochondrial fission, increase in proliferation and apoptosis resistance (Fig. 3E–N).

Because Mfn2's S442 site is also a predicted phosphorylation site for PKA (22) (Supplementary Figure 3A–B), we explored this putative mechanism. Although dysregulation of PKA in PAH is not reported, inactivation of PKA attenuates serotonin-induced PASMC migration (26) and hypoxia-induced pulmonary artery remodeling (27). However, the role of PKA in the proliferation of PASMC is controversial. One study demonstrated the involvement of cAMP/PKA pathway in the antiproliferative effects of prostacyclin analogues in PASMC (28). Furthermore, the PKA pathway also mediates the antiproliferative effect of bone morphogenetic protein 4 (BMP4) on platelet-derived growth factor (PDGF)-induced proliferation and collagen synthesis in PASMC (29). In contrast to PAH, in cancer, the role of PKA and its regulators is clearer. Upregulation of PKA-I isoform is a prognostic biomarker for most human tumors (30). Both PKA and its regulatory subunits are drug targets for cancer therapy (31). Further certainty of the predicted role of PKA in downregulating the expression of Mfn2 comes from our experimental results, which reveal that pharmacological inhibition of PKA upregulates Mfn2 expression and restores a more fused mitochondrial morphology (Fig. 3Q–R). In addition, silencing the functional subunit of PKA (PKA C-α) upregulates the expression of Mfn2, restores mitochondrial network fusion, inhibits cell proliferation and induces apoptosis (Fig. 3T–X). To exclude the possibility that siPKA upregulates Mfn2 by inhibiting mitophagy or inhibiting lysosomes, we examined the effects of silencing PKA C-α on LC3B, a mitophagy marker, and the effects of a lysosomal inhibitor, Bafilomycin A1 on Mfn2 expression. We observed that silencing PKA increased, rather than decreased, mitophagy (Supplementary Figure 5A). Moreover, inhibiting lysosomes reduced Mfn2 expression (Supplementary Figure 5B). Thus, neither reduced mitophagy nor inhibition of lysosomal function can account for the ability of siPKA to increase Mfn2 expression.

A key indicator of the pharmacologic relevance of the S442 phosphorylation is our demonstration of a pathological increase in phosphorylation of Mfn2 at S442 in both PAH PASMC and A549 cells (Fig. 4A–B). Consistent with the proposed mechanism, silencing of

PINK1 suppresses this Mfn2 phosphorylation (Fig. 4C–D). Although PKA expression and activity were not increased in PAH and NSCLC, inhibition of S442 phosphorylation occurs when PKA is knocked down (Fig. 4E). These results taken together may indicate a critical role for both kinases in phosphorylating Mfn2 in PAH and lung cancer.

We also provide evidence that the S442 site of Mfn2 plays a critical role in maintaining the overall stability of the protein. Our results using CP-Mfn2 indicated that phosphorylation at S442 increases proteasomal degradation of Mfn2 protein (Fig. 5A–B and Supplementary Figure 7A–B) whereas the phosphoresistant mutant (PD-Mfn2) stabilizes the protein (Fig. 5A–B and Supplementary Figure 7A–B) and increases its antiproliferative and proapoptotic abilities by causing a cell cycle blockade at the G0/G1 phase (Fig. 5H–K and Fig. 6A–B). In addition, PD-Mfn2 increases pyruvate dehydrogenase activity, suggesting it reverses the Warburg phenomenon (Supplementary Figure 9D). Both wild type and phosphodeficient Mfn2 increase mitochondrial ROS production (Supplementary Figure 9C). These two effects of Mfn2 augmentation suggest metabolic and redox mechanisms by which Mfn2 therapy may regress tumor growth (Fig. 7C–D).

This study further supports the concept that mitochondrial and nuclear division are closely linked in rapidly proliferating cells, as reviewed in (1). Several strategies in the past have exploited the idea of targeting dysregulated mitochondrial dynamics for treating PAH and lung cancer. For example, mitochondrial division may be prevented by the pharmacological inhibition of Drp1 activity using the small molecule GTPase inhibitor, mdivi-1 (32) or more recently by a novel, specific, Drp1's GTPase inhibitor, Drpitor1a (13). Both mdivi-1 and Drpitor1a increase mitochondrial fusion, decrease cell proliferation and enhance apoptosis in PAH PASMC and induce tumor regression in murine xenotransplant models of lung cancer (2, 3, 13). In addition, inducing mitochondrial fusion by augmenting Mfn2 has therapeutic benefits in experimental PAH, in a model of neointimal proliferation induced by balloon injury and in cancers (4, 5, 22). In accordance with these findings, we observed that PD-Mfn2, by superior induction of mitochondrial fusion, caused greater reduction of tumor growth in vivo compared to WT-Mfn2 (Fig. 7A–D).

## Limitations:

Although S442 site of Mfn2 is a predicted PKA phosphorylation site, pharmacological and molecular manipulation of PKA alters the expression of Mfn2 and the downstream cellular effects as would be predicted, a direct link between PKA and the basal downregulation of Mfn2 was not established in this study. Furthermore, the efficacy of PD-Mfn2 in rodent models of PAH was not investigated in this study since the therapeutic efficacy of augmenting Mfn2 in preclinical models of PAH has been reported previously (4).

In conclusion, PINK1 and/or PKA induced phosphorylation of Mfn2 at S442 triggers proteasomal degradation of this fusion mediator. Rendering Mfn2 resistant to phosphorylation at S442 (PD-Mfn2) increases its expression and enhances its fusogenic, antiproliferative and proapoptotic effects and suppresses tumor growth in a xenotransplantation model of lung cancer. Modification of Mfn2 to make it resistant to proteasomal degradation has therapeutic implications for lung cancer and PAH. A schematic representation of the proposed mechanism is shown in Fig. 7E.

## Supplementary Material

Refer to Web version on PubMed Central for supplementary material.

## Acknowledgements:

SLA and his research are supported by Queen's Cardiopulmonary Unit (QCPU). The authors thank Dr. Mamoru Ito (Central Institute for Experimental Animals, Kawasaki, Japan) for providing the BALB/c-Rag2$^{-/-}$IL2R$\gamma$c$^{-/-}$ mice.

Funding Sources:

CIHR Foundation Grant, NIH-RO1-HL071115, 1RC1HL099462, a Tier 1 Canada Research Chair in Mitochondrial Dynamics and the William J Henderson Foundation (SLA), Canadian Vascular Network Scholar Award (AD and DW).

## Nonstandard Abbreviations

| | |
|---|---|
| **Akt** | protein kinase B |
| **BEAS-2B** | a human non-tumorigenic lung epithelial cell line |
| **Drp1** | dynamin-related protein 1 |
| **ERK** | extracellular signal–regulated kinase |
| **GTPase** | a large family of hydrolase enzymes that bind to the nucleotide guanosine triphosphate (GTP) and hydrolyze it to guanosine diphosphate (GDP) |
| **mdivi-1** | mitochondrial division inhibitor 1 |
| **MiD49** | mitochondrial dynamics protein of 49 kDa |
| **MiD51** | mitochondrial dynamics protein of 51 kDa |
| **MFC** | mitochondrial fragmentation count |
| **Mfn1** | mitofusin 1 |
| **Mfn2** | mitofusin 2 |
| **MNF** | mitochondrial networking factor |
| **MTOR** | gene encoding the mammalian target of rapamycin |
| **NHBE** | normal human bronchial epithelial cells |
| **NSCLC** | non-small cell lung cancer |
| **PAH** | pulmonary arterial hypertension |
| **PDH** | pyruvate dehydrogenase |
| **PINK1** | phosphatase and tensin homolog (PTEN)-induced putative kinase 1 |

| | |
|---|---|
| **PASMC** | pulmonary artery smooth muscle cell |
| **PKA** | protein kinase A |
| **ROS** | reactive oxygen species |
| **siRNA** | small interfering RNA |

## References


1. Archer SL (2013) Mitochondrial dynamics--mitochondrial fission and fusion in human diseases. N Engl J Med 369, 2236–2251 [PubMed: 24304053]
2. Marsboom G, Toth PT, Ryan JJ, Hong Z, Wu X, Fang YH, Thenappan T, Piao L, Zhang HJ, Pogoriler J, Chen Y, Morrow E, Weir EK, Rehman J, and Archer SL (2012) Dynamin-related protein 1-mediated mitochondrial mitotic fission permits hyperproliferation of vascular smooth muscle cells and offers a novel therapeutic target in pulmonary hypertension. Circ Res 110, 1484–1497 [PubMed: 22511751]
3. Rehman J, Zhang HJ, Toth PT, Zhang Y, Marsboom G, Hong Z, Salgia R, Husain AN, Wietholt C, and Archer SL (2012) Inhibition of mitochondrial fission prevents cell cycle progression in lung cancer. FASEB journal : official publication of the Federation of American Societies for Experimental Biology 26, 2175–2186 [PubMed: 22321727]
4. Ryan JJ, Marsboom G, Fang YH, Toth PT, Morrow E, Luo N, Piao L, Hong Z, Ericson K, Zhang HJ, Han M, Haney CR, Chen CT, Sharp WW, and Archer SL (2013) PGC1alpha-mediated mitofusin-2 deficiency in female rats and humans with pulmonary arterial hypertension. American journal of respiratory and critical care medicine 187, 865–878 [PubMed: 23449689]
5. Xu K, Chen G, Li X, Wu X, Chang Z, Xu J, Zhu Y, Yin P, Liang X, and Dong L (2017) MFN2 suppresses cancer progression through inhibition of mTORC2/Akt signaling. Sci Rep 7, 41718 [PubMed: 28176801]
6. Wang W, Lu J, Zhu F, Wei J, Jia C, Zhang Y, Zhou L, Xie H, and Zheng S (2012) Pro-apoptotic and anti-proliferative effects of mitofusin-2 via Bax signaling in hepatocellular carcinoma cells. Medical oncology 29, 70–76 [PubMed: 21190094]
7. Cheng X, Zhou D, Wei J, and Lin J (2013) Cell-cycle arrest at G2/M and proliferation inhibition by adenovirus-expressed mitofusin-2 gene in human colorectal cancer cell lines. Neoplasma 60, 620–626 [PubMed: 23906296]
8. Prieto J, Leon M, Ponsoda X, Sendra R, Bort R, Ferrer-Lorente R, Raya A, Lopez-Garcia C, and Torres J (2016) Early ERK1/2 activation promotes DRP1-dependent mitochondrial fission necessary for cell reprogramming. Nature communications 7, 11124
9. Serasinghe MN, Wieder SY, Renault TT, Elkholi R, Asciolla JJ, Yao JL, Jabado O, Hoehn K, Kageyama Y, Sesaki H, and Chipuk JE (2015) Mitochondrial division is requisite to RAS-induced transformation and targeted by oncogenic MAPK pathway inhibitors. Molecular cell 57, 521–536 [PubMed: 25658204]
10. Xu S, Wang P, Zhang H, Gong G, Gutierrez Cortes N, Zhu W, Yoon Y, Tian R, and Wang W (2016) CaMKII induces permeability transition through Drp1 phosphorylation during chronic beta-AR stimulation. Nature communications 7, 13189
11. Chen KH, Dasgupta A, Lin J, Potus F, Bonnet S, Iremonger J, Fu J, Mewburn J, Wu D, Dunham-Snary K, Theilmann AL, Jing ZC, Hindmarch C, Ormiston ML, Lawrie A, and Archer SL (2018) Epigenetic Dysregulation of the Dynamin-Related Protein 1 Binding Partners MiD49 and MiD51 Increases Mitotic Mitochondrial Fission and Promotes Pulmonary Arterial Hypertension: Mechanistic and Therapeutic Implications. Circulation 138, 287–304 [PubMed: 29431643]
12. Dasgupta A, Chen KH, Wu D, Hoskin V, Mewburn J, Lima PDA, Parlow LRG, Hindmarch CCT, Martin A, Sykes EA, Tayade C, Lightbody ED, Madarnas Y, SenGupta SK, Elliott BE, Nicol CJB, and Archer SL (2020) An epigenetic increase in mitochondrial fission by MiD49 and MiD51 regulates the cell cycle in cancer: Diagnostic and therapeutic implications. FASEB journal : official publication of the Federation of American Societies for Experimental Biology 34, 5106–5127 [PubMed: 32068312]

13. Wu D, Dasgupta A, Chen KH, Neuber-Hess M, Patel J, Hurst TE, Mewburn JD, Lima PDA, Alizadeh E, Martin A, Wells M, Snieckus V, and Archer SL (2020) Identification of novel dynamin-related protein 1 (Drp1) GTPase inhibitors: Therapeutic potential of Drpitor1 and Drpitor1a in cancer and cardiac ischemia-reperfusion injury. FASEB J 34, 1447–1464 [PubMed: 31914641]

14. Ryan J, Dasgupta A, Huston J, Chen KH, and Archer SL (2015) Mitochondrial dynamics in pulmonary arterial hypertension. Journal of molecular medicine 93, 229–242 [PubMed: 25672499]

15. Kashatus JA, Nascimento A, Myers LJ, Sher A, Byrne FL, Hoehn KL, Counter CM, and Kashatus DF (2015) Erk2 phosphorylation of Drp1 promotes mitochondrial fission and MAPK-driven tumor growth. Molecular cell 57, 537–551 [PubMed: 25658205]

16. Tian L, Potus F, Wu D, Dasgupta A, Chen KH, Mewburn J, Lima P, and Archer SL (2018) Increased Drp1-Mediated Mitochondrial Fission Promotes Proliferation and Collagen Production by Right Ventricular Fibroblasts in Experimental Pulmonary Arterial Hypertension. Front Physiol 9, 828 [PubMed: 30042687]

17. Huang CY, Chiang SF, Chen WT, Ke TW, Chen TW, You YS, Lin CY, Chao KSC, and Huang CY (2018) HMGB1 promotes ERK-mediated mitochondrial Drp1 phosphorylation for chemoresistance through RAGE in colorectal cancer. Cell Death Dis 9, 1004 [PubMed: 30258050]

18. Cereghetti GM, Stangherlin A, Martins de Brito O, Chang CR, Blackstone C, Bernardi P, and Scorrano L (2008) Dephosphorylation by calcineurin regulates translocation of Drp1 to mitochondria. Proceedings of the National Academy of Sciences of the United States of America 105, 15803–15808 [PubMed: 18838687]

19. Chen Y, and Dorn GW 2nd. (2013) PINK1-phosphorylated mitofusin 2 is a Parkin receptor for culling damaged mitochondria. Science 340, 471–475 [PubMed: 23620051]

20. Chen KH, Dasgupta A, Ding J, Indig FE, Ghosh P, and Longo DL (2014) Role of mitofusin 2 (Mfn2) in controlling cellular proliferation. FASEB journal : official publication of the Federation of American Societies for Experimental Biology 28, 382–394 [PubMed: 24081906]

21. Potus F, Ruffenach G, Dahou A, Thebault C, Breuils-Bonnet S, Tremblay E, Nadeau V, Paradis R, Graydon C, Wong R, Johnson I, Paulin R, Lajoie AC, Perron J, Charbonneau E, Joubert P, Pibarot P, Michelakis ED, Provencher S, and Bonnet S (2015) Downregulation of MicroRNA-126 Contributes to the Failing Right Ventricle in Pulmonary Arterial Hypertension. Circulation 132, 932–943 [PubMed: 26162916]

22. Chen KH, Guo X, Ma D, Guo Y, Li Q, Yang D, Li P, Qiu X, Wen S, Xiao RP, and Tang J (2004) Dysregulation of HSG triggers vascular proliferative disorders. Nature cell biology 6, 872–883 [PubMed: 15322553]

23. Mashima T, Seimiya H, Chen Z, Kataoka S, and Tsuruo T (1998) Apoptosis resistance in tumor cells. Cytotechnology 27, 293–308 [PubMed: 19002800]

24. Leboucher GP, Tsai YC, Yang M, Shaw KC, Zhou M, Veenstra TD, Glickman MH, and Weissman AM (2012) Stress-induced phosphorylation and proteasomal degradation of mitofusin 2 facilitates mitochondrial fragmentation and apoptosis. Molecular cell 47, 547–557 [PubMed: 22748923]

25. Dasgupta A, Chen KH, Munk RB, Sasaki CY, Curtis J, Longo DL, and Ghosh P (2015) Mechanism of Activation-Induced Downregulation of Mitofusin 2 in Human Peripheral Blood T Cells. Journal of immunology 195, 5780–5786

26. Day RM, Agyeman AS, Segel MJ, Chevere RD, Angelosanto JM, Suzuki YJ, and Fanburg BL (2006) Serotonin induces pulmonary artery smooth muscle cell migration. Biochem Pharmacol 71, 386–397 [PubMed: 16316635]

27. He Y, Zuo C, Jia D, Bai P, Kong D, Chen D, Liu G, Li J, Wang Y, Chen G, Yan S, Xiao B, Zhang J, Piao L, Li Y, Deng Y, Li B, Roux PP, Andreasson KI, Breyer RM, Su Y, Wang J, Lyu A, Shen Y, and Yu Y (2020) Loss of DP1 Aggravates Vascular Remodeling in Pulmonary Arterial Hypertension via mTORC1 Signaling. American journal of respiratory and critical care medicine 201, 1263–1276 [PubMed: 31917615]

28. Yang J, Li X, Al-Lamki RS, Southwood M, Zhao J, Lever AM, Grimminger F, Schermuly RT, and Morrell NW (2010) Smad-dependent and smad-independent induction of id1 by prostacyclin analogues inhibits proliferation of pulmonary artery smooth muscle cells in vitro and in vivo. Circulation research 107, 252–262 [PubMed: 20522807]

29. Cai P, Kovacs L, Dong S, Wu G, and Su Y (2017) BMP4 inhibits PDGF-induced proliferation and collagen synthesis via PKA-mediated inhibition of calpain-2 in pulmonary artery smooth muscle cells. American journal of physiology. Lung cellular and molecular physiology 312, L638–L648 [PubMed: 28235949]

30. Caretta A, and Mucignat-Caretta C (2011) Protein kinase a in cancer. Cancers 3, 913–926 [PubMed: 24212646]

31. Sapio L, Di Maiolo F, Illiano M, Esposito A, Chiosi E, Spina A, and Naviglio S (2014) Targeting protein kinase A in cancer therapy: an update. EXCLI J 13, 843–855 [PubMed: 26417307]

32. Cassidy-Stone A, Chipuk JE, Ingerman E, Song C, Yoo C, Kuwana T, Kurth MJ, Shaw JT, Hinshaw JE, Green DR, and Nunnari J (2008) Chemical inhibition of the mitochondrial division dynamin reveals its role in Bax/Bak-dependent mitochondrial outer membrane permeabilization. Developmental cell 14, 193–204 [PubMed: 18267088]

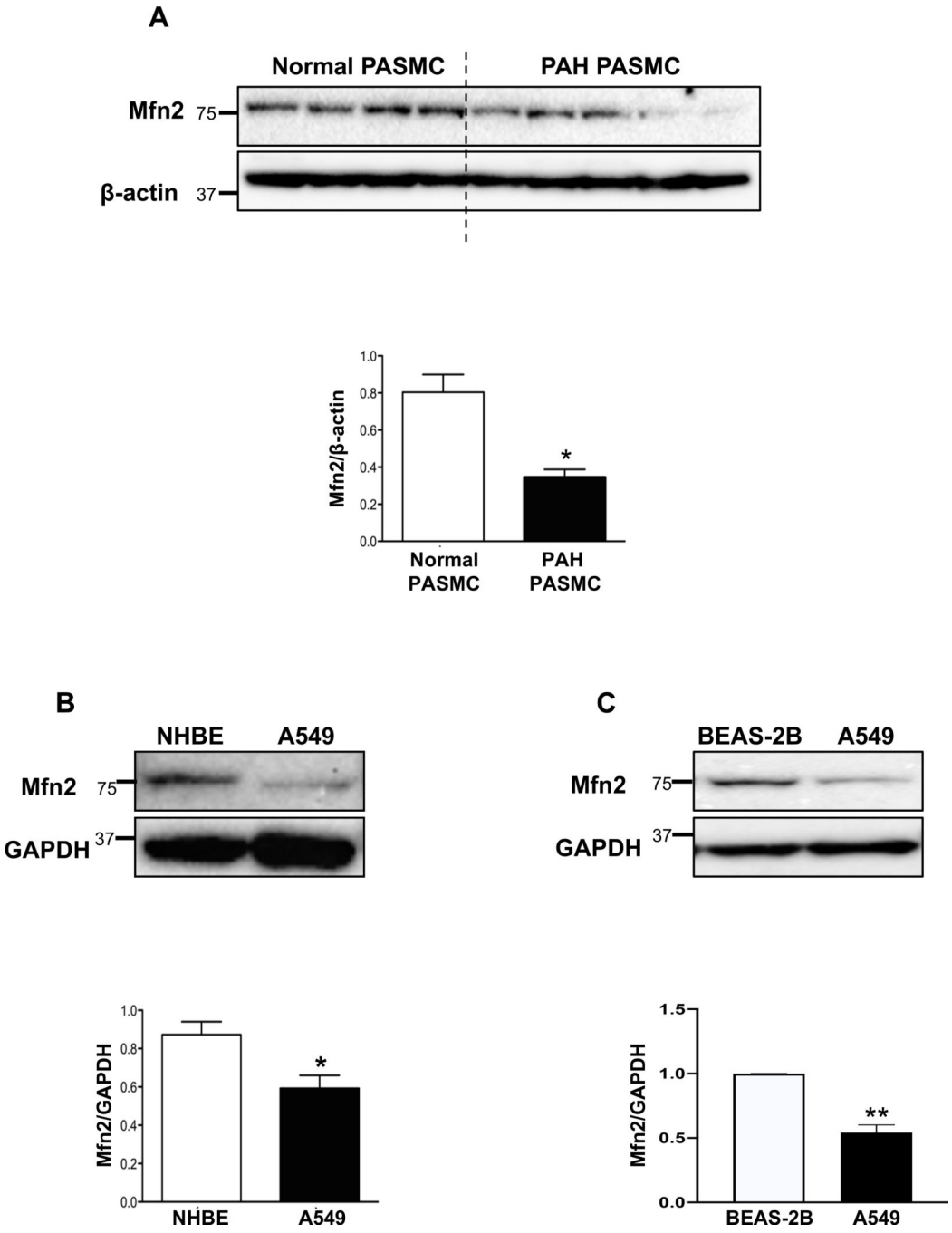


**Figure 1: Pathological downregulation of Mfn2 in human PAH PASMC and the NSCLC cell line, A549.**

A) Representative immunoblots and densitometry demonstrating decreased expression of Mfn2 protein in human PAH PASMC (n=5) vs normal PASMC (n=4). β-actin was used as a loading control. $*P < 0.05$.

B) Representative immunoblots and densitometry demonstrating decreased expression of Mfn2 protein in a NSCLC cell line, A549 vs normal human bronchial epithelial cells, NHBE (n=3). GAPDH was used as the loading control. $*P < 0.05$.

C) Representative immunoblots and densitometry demonstrating decreased expression of Mfn2 protein in a NSCLC cell line, A549 vs non-neoplastic bronchial epithelial cells, BEAS-2B (n=3). GAPDH was used as the loading control. $^{**}P < 0.01$.

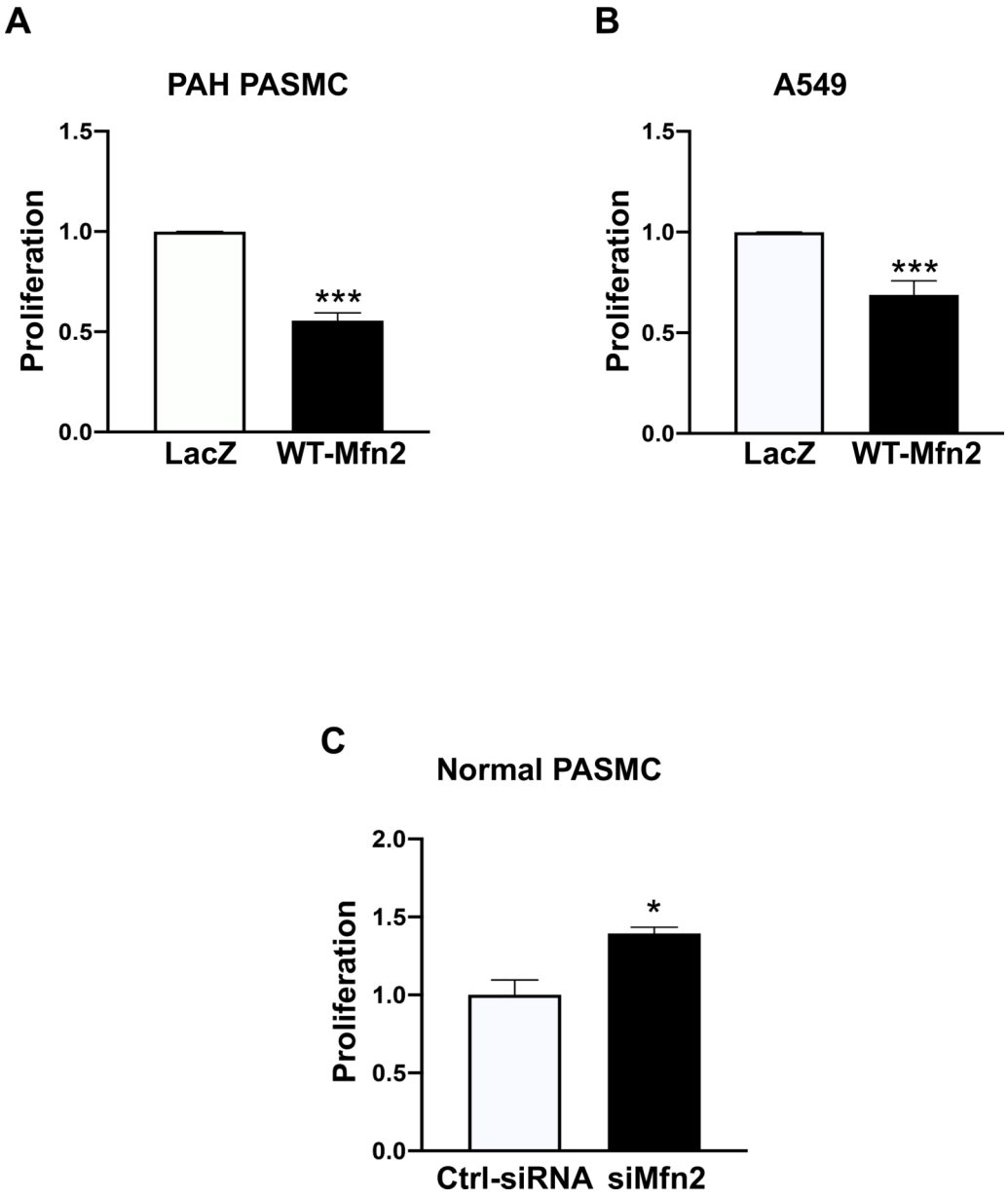


**Figure 2: Augmenting Mfn2 suppresses proliferation in PAH PASMC and A549 cells whereas silencing Mfn2 stimulates proliferation in normal PASMC.**

A) PAH PASMC were infected with adenoviruses carrying WT-Mfn2 or LacZ genes. Cell proliferation was analyzed by Click-iT EdU flow cytometry assay kit 72 hours following infection (n=3/group). ***$P < 0.001$.

B) A549 cells were infected with adenoviruses carrying WT-Mfn2 or LacZ genes. Cell proliferation was analyzed by Click-iT EdU flow cytometry assay kit 72 hours following infection (n=3/group). ***$P < 0.001$.

C) Normal PASMC were transfected with Ctrl-siRNA or siMfn2. Cell proliferation was analyzed by Click-iT EdU flow cytometry assay kit 72 hours following transfection (n=3/group). *$P < 0.05$.

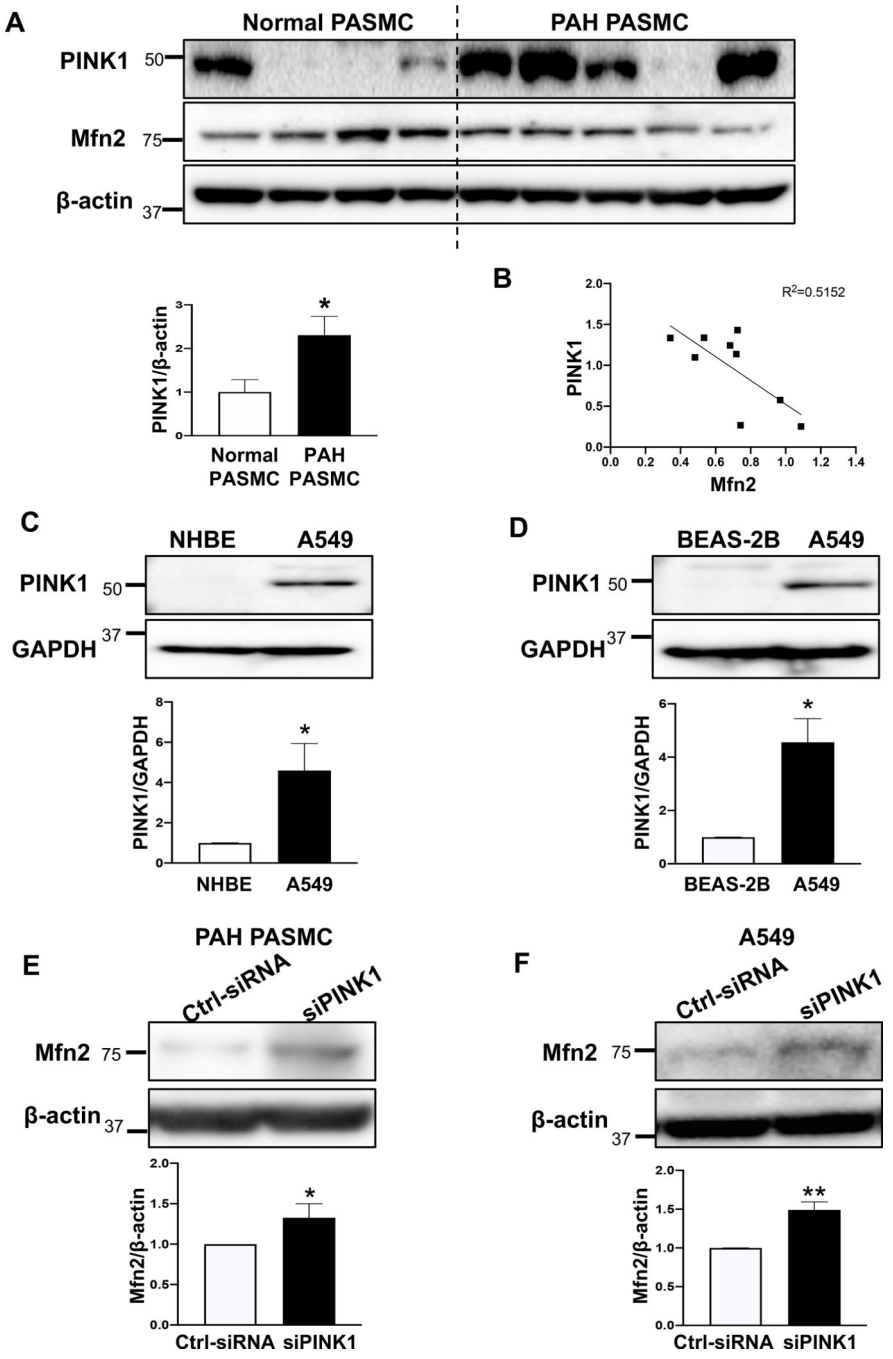

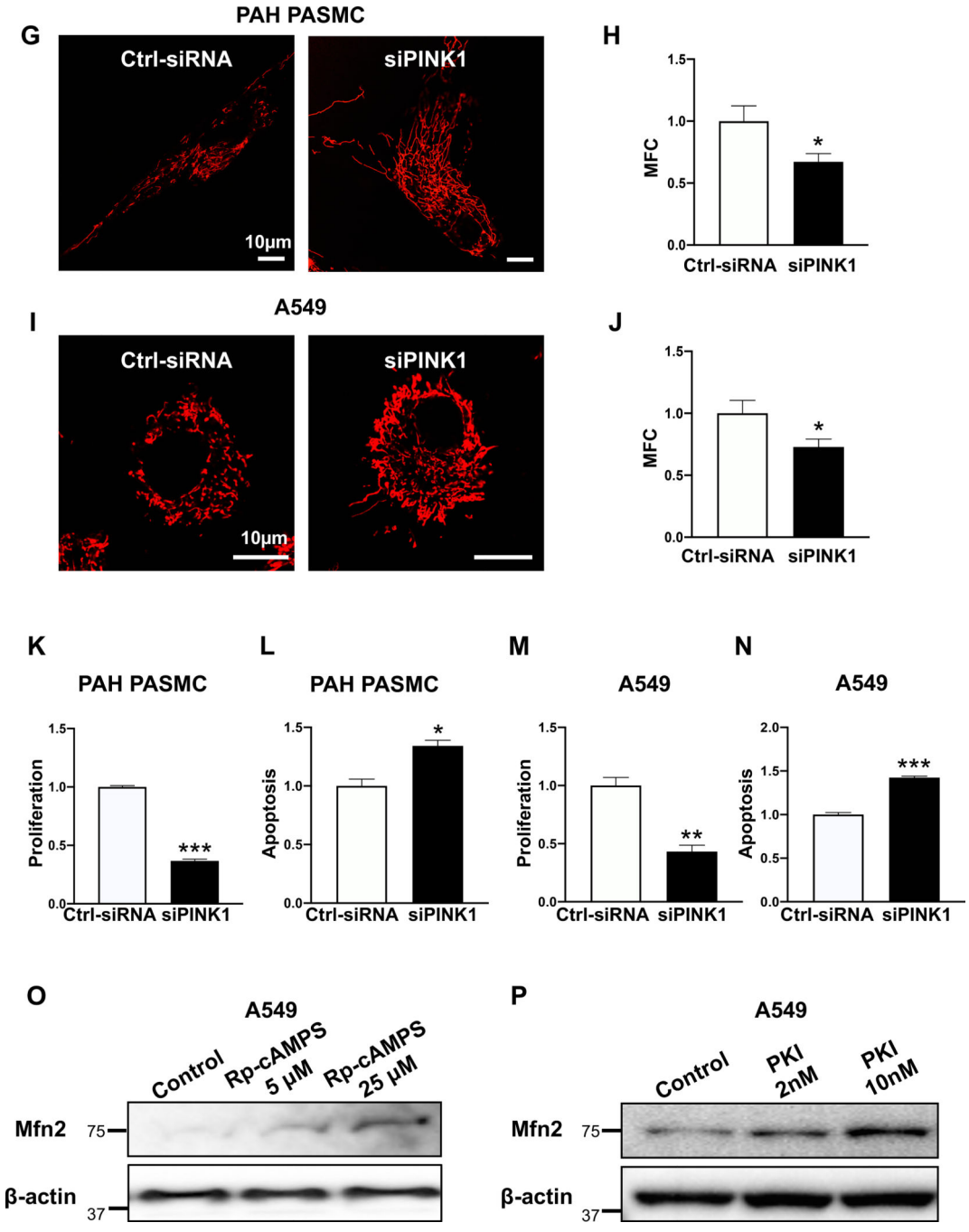

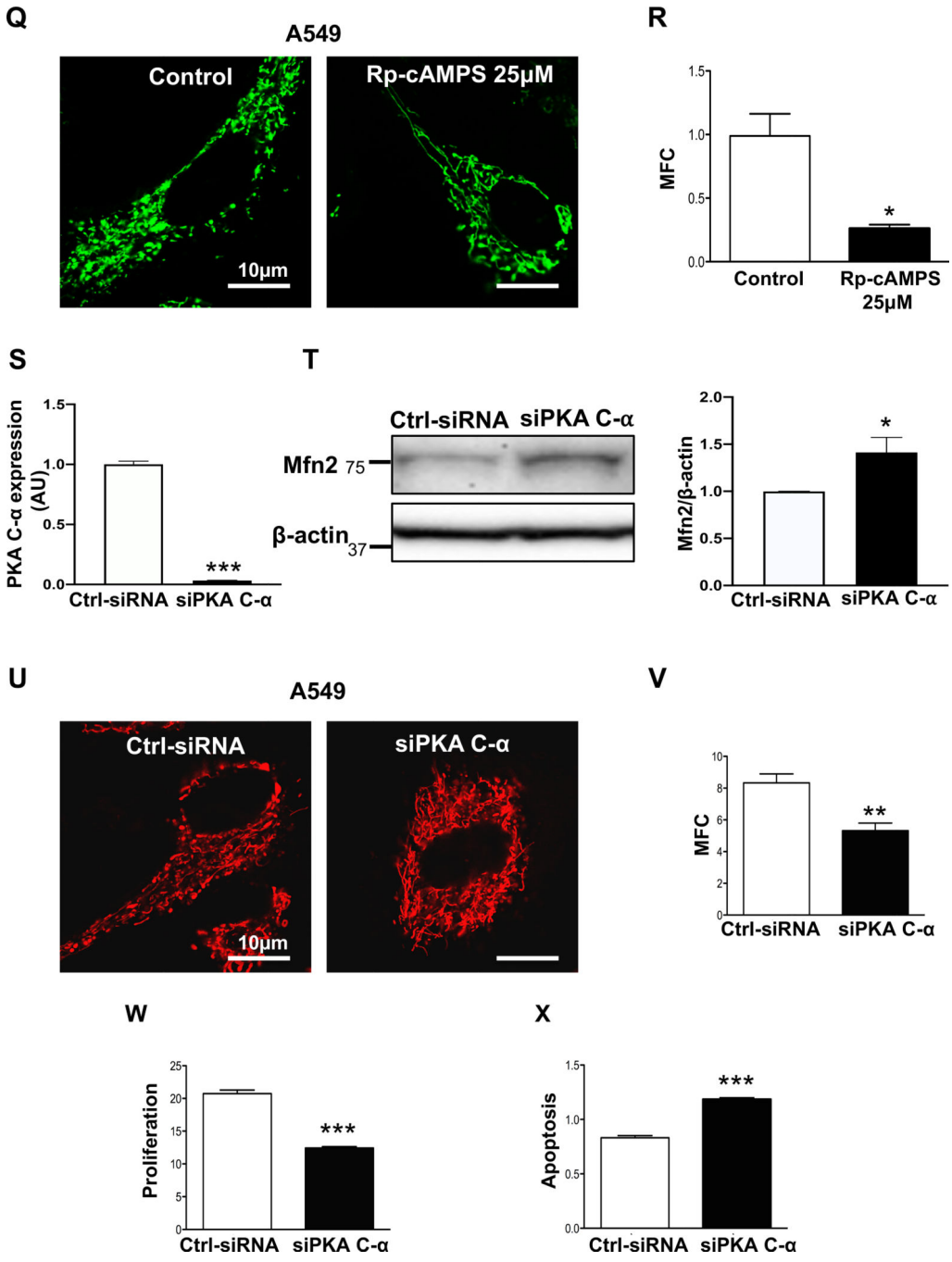


**Figure 3: PINK1 is pathologically upregulated in PAH PASMC and A549 cells and silencing PINK1 or PKA restores Mfn2 expression, rescues mitochondrial morphology, inhibits cell proliferation and induces apoptosis.**

**A) Representative immunoblots and densitometry demonstrating increased protein expression of PINK1 in human PAH PASMC vs normal human PASMC** (n=4 for normal PASMC and n=5 for PAH PASMC). β-actin was used as a loading control. **P* < 0.05.

**B) Mfn2 expression is inversely correlated to PINK1 expression.** Correlation analysis showing that expression level of Mfn2 and PINK1 are inversely correlated (n=9). $R^2$=0.5152.

**C-D) Representative immunoblots and densitometry demonstrating increased protein expression of PINK1 in A549 as compared to: C) NHBE or D) BEAS-2B** (n=3). GAPDH was used as the loading control. *$P < 0.05$.

**E-F) Silencing PINK1 restores the expression of Mfn2 protein in PAH PASMC and A549 cells. Representative immunoblots and densitometry showing upregulation of Mfn2 in: E) PAH PASMC and F) A549 cells.** Cells were transfected with Ctrl-siRNA or siPINK1. Cells were harvested for immunoblot analyses 48 hours following transfection (n=3). β-actin was used as the loading control. *$P < 0.05$, **$P < 0.01$.

G-J) Silencing PINK1 rescues mitochondrial morphology in PAH PASMC and A549 cells.

G) PAH PASMC transfected with Ctrl-siRNA or siPINK1 for 48 hours. Cells were then loaded with the potentiometric dye TMRM (red) and imaged with a confocal microscope to assess the mitochondrial network structure. Scale bar: 10 μm.

H) Mitochondrial fragmentation count (MFC) was calculated in PAH PASMC following PINK1 knockdown (n=13/group). *$P < 0.05$.

I) A549 cells transfected with Ctrl-siRNA or siPINK1 for 48 hours. Cells were then loaded with the potentiometric dye TMRM (red) and imaged with confocal microscope to assess the mitochondrial network structure. Scale bar: 10 μm.

J) Mitochondrial fragmentation count (MFC) was calculated in A549 cells following PINK1 knockdown. (n=10–12/group). *$P < 0.05$.

K-N) Silencing PINK1 inhibits cell proliferation and induces apoptosis in PAH PASMC and A549 cells.

**K) Silencing PINK1 inhibits cell proliferation in PAH PASMC.** PAH PASMC were transfected with either Ctrl-siRNA or siPINK1. Cell proliferation was analyzed by Click-iT EdU flow cytometry assay kit 72 hours following transfection (n=3/group). ***$P < 0.001$.

**L) Silencing PINK1 induces apoptosis in PAH PASMC.** PAH PASMC were transfected with either Ctrl-siRNA or siPINK1. The cells were labeled with Annexin $V^{FITC}$ and PI and assessed by flow cytometry analyses 72 hours post transfection (n=3/group). *$P < 0.05$.

**M) Silencing PINK1 inhibits cell proliferation in A549 cells.** A549 cells were transfected with either Ctrl-siRNA or siPINK1. Cell proliferation was analyzed by Click-iT EdU flow cytometry assay kit 72 hours following transfection (n=3/group). **$P < 0.01$.

**N) Silencing PINK1 induces apoptosis in A549 cells.** A549 cells were transfected with either Ctrl-siRNA or siPINK1 for 72 hours. The cells were labeled with Annexin $V^{FITC}$ and PI and assessed by flow cytometry analyses 72 hours post transfection (n=3/group). ***$P < 0.001$.

O-R) Pharmacological inhibition of PKA upregulates Mfn2 and induces mitochondrial fusion.

O) Representative immunoblots showing upregulation of Mfn2 in A549 cells. A549 cells were treated with or without PKA inhibitor Rp-cAMPS for 48 hours. β-actin was used as the loading control.

P) Representative immunoblots showing upregulation of Mfn2 in A549 cells. A549 cells were treated with or without PKA specific inhibitor (PKI) for 48 hours. β-actin was used as the loading control.

Q) A549 cells were treated with or without the PKA inhibitor (Rp-cAMPS) for 48 hours. Cells were stained with MitoTracker Green and imaged with confocal microscope to assess the mitochondrial network structure. Scale bar: 10μm.

R) Mitochondrial fragmentation count (MFC) was calculated in A549 cells following inhibition of PKA by Rp-cAMPs (n=13–22/group). $*P < 0.05$.

S-X) Silencing PKA upregulates Mfn2, induces mitochondrial fusion, inhibits cell proliferation and increases apoptosis rate.

S) Knockdown efficiency of siPKA C-α. RNA analyses with qRT-PCR was performed 48 hours after transfection (n=3/group). $***P < 0.001$.

T) Representative immunoblots showing upregulation of Mfn2 following silencing of PKA C-α in A549 cells. (n=3). β-actin was used as the loading control. $*P < 0.05$.

U) A549 cells were transfected with Ctrl-siRNA or siPKA C-α for 48 hours. Cells were loaded with the potentiometric dye TMRM (red) and imaged with confocal microscope to assess the mitochondrial network structure. Scale bar: 10 μm.

V) Mitochondrial fragmentation count (MFC) was calculated in A549 cells following PKA C-α knockdown (n=9–12/group). $**P < 0.01$.

W) A549 cells were transfected with either Ctrl-siRNA or siPKA C-α. Cell proliferation was analyzed by Click-iT EdU flow cytometry assay kit 72 hours following transfection (n=3/group). $***P < 0.001$.

X) A549 cells were transfected with either Ctrl-siRNA or siPKA C-α for 72 hours. The cells were labeled with Annexin $V^{FITC}$ and PI and assessed by flow cytometry analyses 72 hours post transfection (n=3/group). $***P < 0.001$.

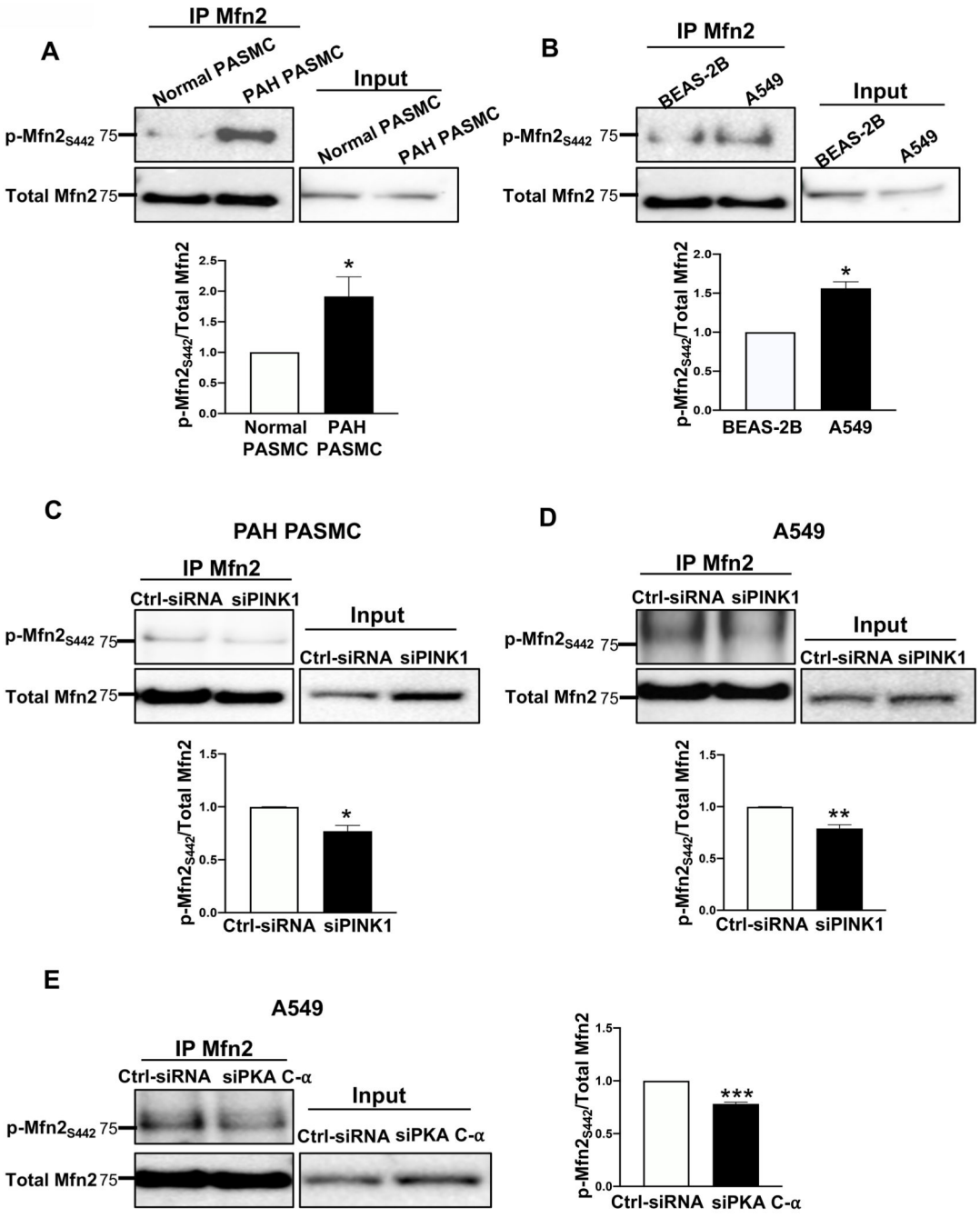


**Figure 4: Mfn2 is hyperphosphorylated in PAH PASMC and A549 cells by PINK1 and PKA.**

A-B) Phosphorylation of Mfn2 at S442 is increased in PAH PASMC and A549 cells.

A) Representative immunoblots and densitometry of immunoprecipitation reaction performed with cell lysates (1000 μg) from normal PASMC and PAH PASMC. Immunoprecipitation reactions were performed with anti-Mfn2 antibody and immunoblotted with p-Mfn2$_{S442}$ (top panel) and total Mfn2 antibody (bottom panel). Total cell extracts (50 μg) were used as positive control for expression of Mfn2 (n=3/group). *$P < 0.05$.

B) Representative immunoblots and densitometry of immunoprecipitation reaction performed with cell lysates (1000 μg) from the non-neoplastic cells, BEAS-2B, and NSCLC cells, A549. Immunoprecipitation reactions were performed with anti-Mfn2 antibody and immunoblotted with p-Mfn2$_{S442}$ (top panel) and total Mfn2 antibody (bottom panel). Total cell extracts (50 μg) were used as positive control for expression of Mfn2 (n=3/group). *$P$ < 0.05.

C-E) Phosphorylation of Mfn2 at S442 is inhibited following PINK1 and PKA C-α silencing in PAH PASMC and A549 cells.

C) Representative immunoblots and densitometry of immunoprecipitation reactions performed with cell lysates (1000 μg) from PAH PASMC transfected either with Ctrl-siRNA or siPINK1. Immunoprecipitation reactions were performed with anti-Mfn2 antibody and immunoblotted with p-Mfn2$_{S442}$ (top panel) and total Mfn2 antibody (bottom panel). Total cell extracts (50 μg) were used as positive control for expression of Mfn2 (n=3/group). *$P$ < 0.05.

D) Representative immunoblots and densitometry of immunoprecipitation reactions performed with cell lysates (1000 μg) from A549 cells transfected either with Ctrl-siRNA or siPINK1. Immunoprecipitation reactions were performed with anti-Mfn2 antibody and immunoblotted with p-Mfn2$_{S442}$ (top panel) and total Mfn2 antibody (bottom panel). Total cell extracts (50 μg) were used as positive control for expression of Mfn2 (n=3/group). **$P$ < 0.01.

E) Representative immunoblots and densitometry of immunoprecipitation reactions performed with cell lysates (1000 μg) from A549 cells transfected either with Ctrl-siRNA or siPKA C-α. Cell lysates (1000 μg) were immunoprecipitated with anti-Mfn2 antibody and immunoblotted with p-Mfn2$_{S442}$ (top panel) and total Mfn2 antibody (bottom panel). Total cell extracts (50 μg) were used as positive control for expression of Mfn2. (n=3/group). ***$P$ < 0.001.

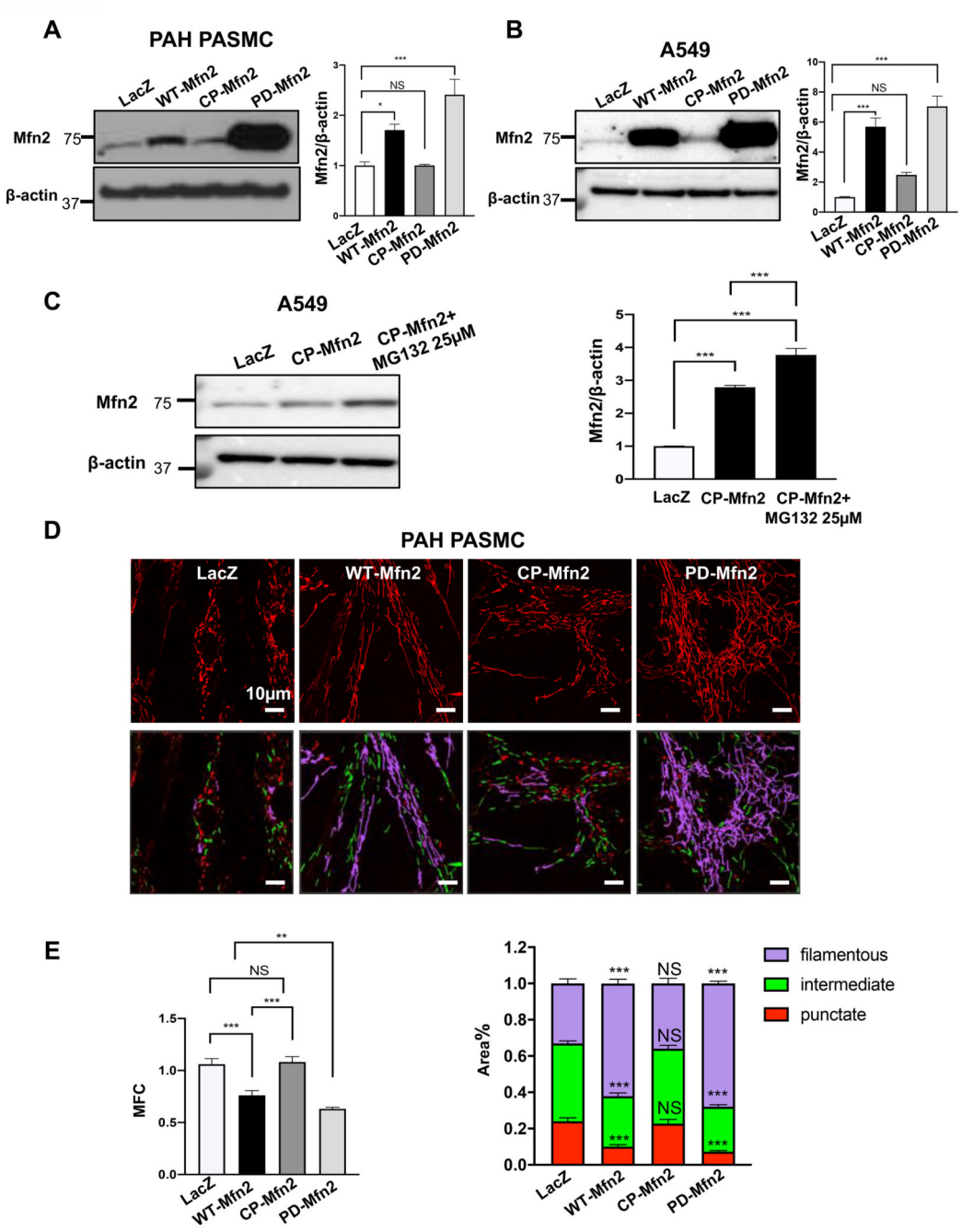

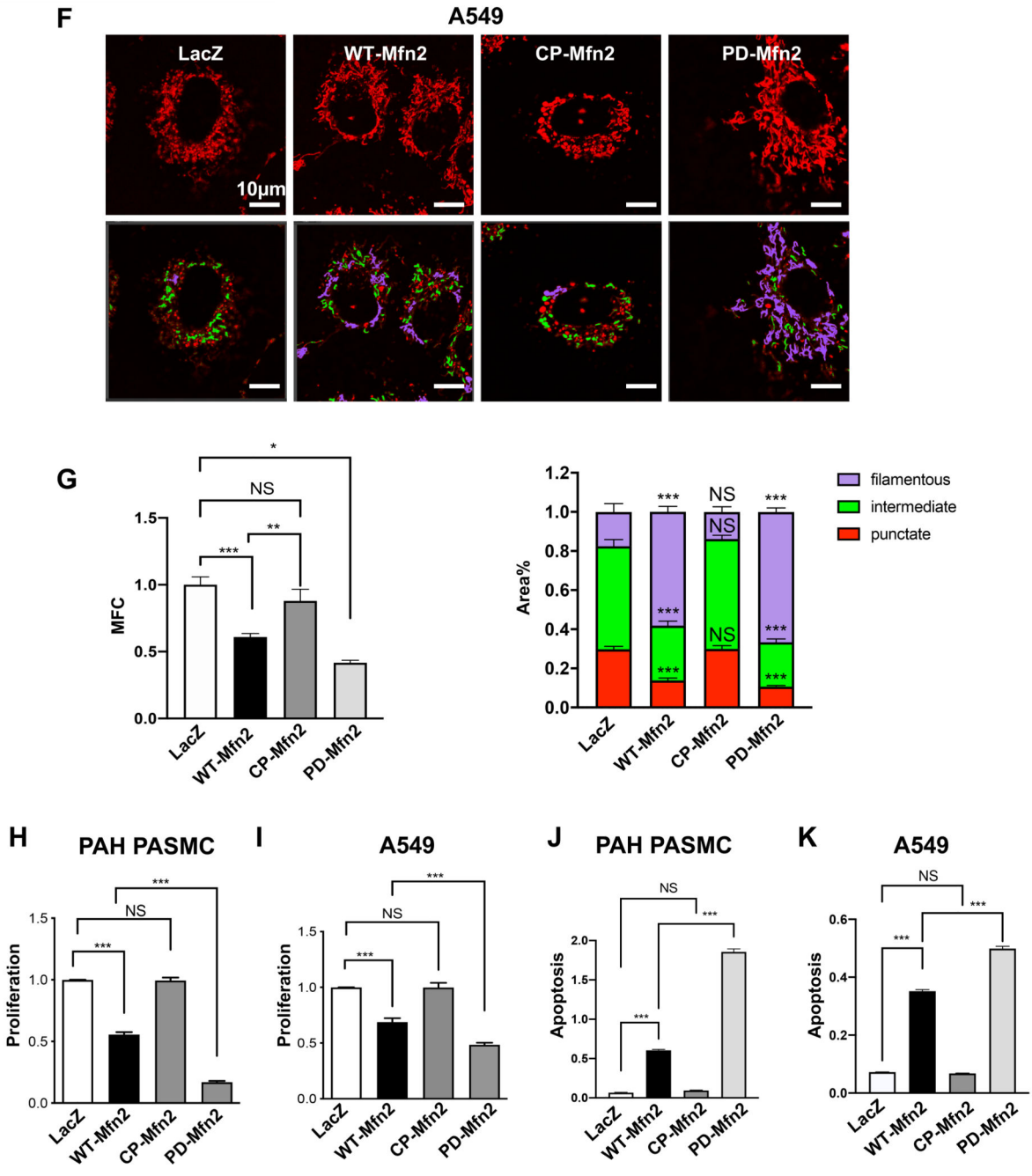


**Figure 5: A phosphodeficient construct of Mfn2 (PD-Mfn2) results in higher expression of Mfn2 than WT-Mfn2, while decreased expression of Mfn2 by CP-Mfn2 is reversed by proteasomal blockade. PD-Mfn2 best suppresses cell proliferation and induces higher rate of apoptosis than WT-Mfn2.**

A-B) Representative immunoblots and densitometries demonstrating increased protein expression of PD-Mfn2.

A) PAH PASMC and B) A549 cells were infected with adenovirus carrying different Mfn2 constructs. Adenovirus carrying LacZ gene was used as a control. Cells were harvested for

immunoblot analyses 48 hours following adenoviral infection. β-actin was used as the loading control (n=3/group). *$P < 0.05$, ***$P < 0.001$, NS, not significant.

**C) Degradation of Mfn2 by CP-Mfn2 is blocked by proteasomal inhibition.** Representative immunoblots and densitometry showing increased expression of Mfn2 by CP-Mfn2 following proteasomal blockade. A549 cells were infected by adenovirus carrying indicated Mfn2 constructs. CP-Mfn2 overexpressed cells were treated with or without a proteasome inhibitor, MG132 (25 μM) for 8 hours before harvesting. β-actin was used as the loading control (n=3/group). ***$P < 0.001$.

D-G) PD-Mfn2 increased mitochondrial fusion.

D) PAH PASMC cells were infected by adenovirus carrying indicated Mfn2 constructs. After 48 hours of infection, the cells were loaded with the potentiometric dye TMRM (red) and imaged with a confocal microscope to assess the mitochondrial network structure. Red, green and purple showing punctate, intermediate and filamentous mitochondria respectively. Scale bar: 10μm.

E) Mitochondrial fragmentation count (MFC) was calculated in PAH PASMC (n=20–59/group). **$P < 0.01$, ***$P < 0.001$, NS, not significant.

F) A549 cells were infected by adenovirus carrying indicated Mfn2 constructs. After 48 hours of infection, the cells were loaded with the potentiometric dye TMRM (red) and imaged with confocal microscope to assess the mitochondrial network structure. Red, green and purple showing punctate, intermediate and filamentous mitochondria respectively. Scale bar: 10μm.

G) Mitochondrial fragmentation count (MFC) was calculated in A549 cells (n=19–21/group). *$P < 0.05$, **$P < 0.01$, ***$P < 0.001$, NS, not significant.

**H-I) PD-Mfn2 better inhibits cell proliferation in H) PAH PASMC and I) A549 cells.** The cells were infected with adenovirus carrying different Mfn2 constructs. Adenovirus carrying LacZ gene was used as a control. Cell proliferation was analyzed by Click-iT EdU flow cytometry assay kit 72 hours following infection (n=4/group). ***$P < 0.001$; NS, not significant.

**J-K) PD-Mfn2 induces higher rate of apoptosis in J) PAH PASMC and K) A549 cells.** The cells were infected with adenovirus carrying different Mfn2 constructs. Adenovirus carrying LacZ gene was used as a control. Apoptosis assay was performed 72 hours following infection by Cell Death ELISA assay (n=4/group). ***$P < 0.001$, NS, not significant.

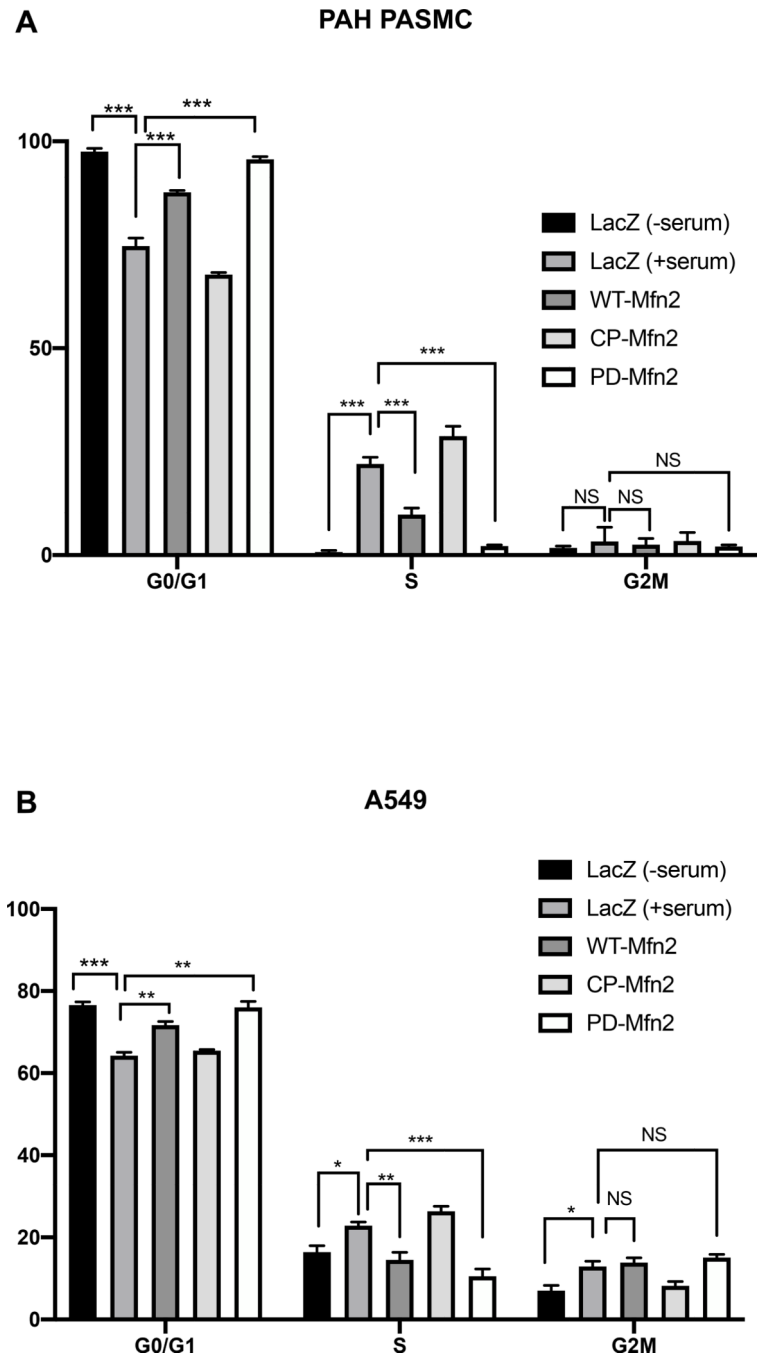


**Figure 6. PD-Mfn2 blocks cell cycle at G0/G1 phase in A) PAH PASMC and B) A549 cells.**
The cells were overexpressed with the indicated Mfn2 constructs by adenoviral infection. The cells were serum starved for 48 hours and stimulated for 24 hours with 15% FBS for PAH PASMC and for 20 hours with 10% FBS for A549 cells. Cell cycle distribution was accessed by propidium iodide staining followed by flowcytometry (n=3/group). $*P < 0.05$, $**P < 0.01$, $***P < 0.001$, NS, not significant.

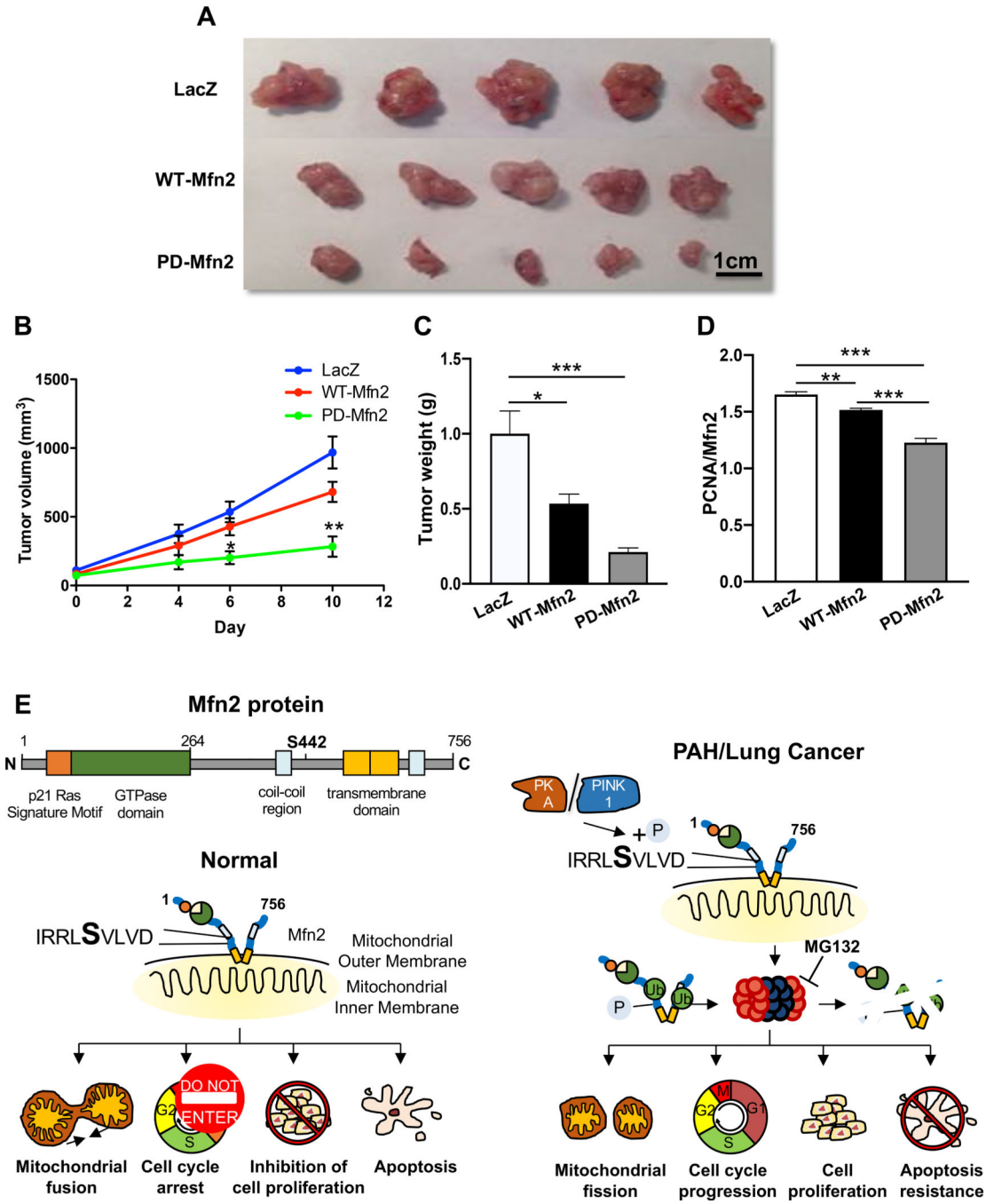


**Figure 7. Overexpression of Mfn2 suppresses tumor growth.**

A) Representative images of excised A549 tumor xenografts from mice that were treated with Adv-LacZ, Adv-WT-Mfn2 or Adv-PD-Mfn2. Scale bar: 1cm.

B) Tumor growth rate assessed overtime in mice as calculated volume (n=5–7/group). Therapeutic interventions of Adv-LacZ, Adv-WT-Mfn2 or Adv-PD-Mfn2 were applied 2 weeks after tumor implantations. *$P < 0.05$, **$P < 0.01$.

C) Weight of excised tumors from animals that were treated with Adv-LacZ, Adv-WT-Mfn2 or Adv-PD-Mfn2. Tumors were excised and weighed after 9 days of treatment (5–7 tumors/group). *$P < 0.05$, ***$P < 0.001$.

D) Quantification of PCNA/Mfn2 ratio showing superior inhibition of tumor growth by PD-Mfn2 relative to WT-Mfn2 (n=12–15 fields/group). **$P < 0.01$, ***$P < 0.001$.

E) Graphical representation of the proposed mechanism of Mfn2 degradation following S442 phosphorylation and its cellular consequences in cells from normal vs hyperproliferative disease origin.